Electronic Supplementary Material (ESI) for New Journal of Chemistry.

Supporting Information

When Ring Makes the Difference: Coordination Properties of Cu^{2+}/Cu^{+} Complexes with Sulfur-Pendant Polyazamacrocycles for Radiopharmaceutical Applications

Marianna Tosato[1], Matteo Pelosato[1], Sara Franchi[1], Abdirisak Ahmed Isse[1], Nóra Veronica May[2], Giordano Zanoni[1], Fabrizio Mancin[1], Paolo Pastore[1], Denis Badocco[1], Mattia Asti[3], Valerio Di Marco[1,*]

[1] Department of Chemical Sciences, University of Padova, 35131 Padova, Italy

[2] Centre for Structural Science, Research Centre for Natural Sciences, 1117 Budapest, Hungary

[3] Radiopharmaceutical Chemistry Section, Nuclear Medicine Unit, AUSL-IRCCS di Reggio Emilia, 42122 Reggio Emilia, Italy

***Corresponding author**: valerio.dimarco@unipd.it

Description of the NMR Spectra of the Free Ligands

The ^{1}H-NMR spectra of TACD3S, TRI4S and TE4S and the ^{1}H chemical shift variations as a function of pH are shown in **Fig. S2** - **S4** and **Fig. S5** - **S7**. The signal assignments, supported by bidimensional spectra of **Fig. S8** - **S11**, are reported in **Tables S1** - **S3**. Chemical shift values in water differ from those in $CDCl_3$ (see Experimental Section) due to the solvent effects and the different ligand protonation states.

For TACD3S, at the most acidic pH, the S-bound methyl and methylenic protons resonate as a singlet and a triplet at 2.15 and 2.92 ppm, respectively (**Fig. S2** and **Table S1**). Both the ring and side-arms nitrogen-bound protons resonate as a triplet at 3.55 and 3.49 ppm, respectively, while the methylenic protons of the ring appear as a quintet a 2.33 ppm. Upon increasing the pH, no significant shifts were detected for the SCH_3 signals as they are far from the (de)protonation sites (**Fig. S2**), whereas all the other resonances shift upfield because of the increase of the electron density on the nitrogens after their deprotonations (**Fig. S2** and **S5**). The same behaviour was observed for TRI4S and TE4S, too.

In TRI4S, the molecular asymmetry generated from the propyl chain induces the splitting of the signals of the side arms at the lowest investigated pH. According to the TOCSY spectra (**Fig. S8**), the SCH_3 protons resonate as two singlets at 2.16 and 2.17 ppm (an enlargement of the SCH_3 signals is shown in **Fig. S12**), the SCH_2 protons as two triplets at 2.87 and 2.93 ppm and the NCH_2 ones as two triplets at 3.21 and 3.50 ppm. The latter signal is overlapped with those of the N-bound ^{1}H of the propyl chain and half of the methylenic protons located on opposite sides of the ring (and equal two by two through the σ_v' symmetry plane); the second half of the latter resonates as a triplet at 3.67 ppm. The NCH_2 ^{1}H opposite to the propyl chain are as well equivalent due to the σ_v' symmetry plane. These protons and the CH_2 ones laying on σ_v' resonate as a singlet at 3.34 ppm and a non-splitted multiplet at 2.25 ppm, respectively. At higher pH, the spectra become complicated as all the SCH_2 and NCH_2 signals overlap, making the exact attribution impossible.

Due to the higher symmetry of TE4S with respect to TRI4S, the signals in the ^{1}H NMR spectra of the former are less complicated at acidic pH while a similar coalescence is observed at basic pH (**Fig. S4** and **Table S3**).

For all the investigated ligands, the N-bound methylenic protons of the ring experience a greater chemical shift variation than those of the side chains when the pH was increased from the most acidic to the most basic (*e.g.* $\Delta\delta^{NCH_2}{}_{, ring} \approx 0.7$ ppm *vs.* $\Delta\delta^{NCH_2}{}_{, arms} \approx 0.5$ ppm for TACD3S and TE4S). The same effect is also observed when the methylenic protons of the ring are compared with those bound to S (*e.g.* $\Delta\delta^{CH_2}{}_{, ring} \approx 0.4$ ppm *vs.* $\Delta\delta^{SCH_2}{}_{, arms} \approx 0.1$ ppm for TACD3S) despite being at the same distance from the protonation sites. This effect might be related to the relaxation of the structural constrain, caused by the H^+-H^+ repulsions, after

the deprotonation: this is higher for the ring than for the side chains because the latter are not confined into a cyclic structure.

Table S1. Chemical shift, multiplicity, relative integral, and ^{1}H resonance assignments for TACD3S. Data were taken from **Fig. S2**.

Species	δ [ppm]	Multiplicity	Relative integral	Assignation
L	1.51 - 1.71	m	6	CH_2 ring
	2.15	s	9	SCH_3
	2.43 - 2.83	m	24	SCH_2 + NCH_2 ring + NCH_2 arms
HL^+	1.85 - 1.93	m	6	CH_2 ring
	2.16	s	9	SCH_3
	2.79	t	6	SCH_2
	2.83 - 2.93	m	12	NCH_2 ring
	2.93 - 3.01	m	6	NCH_2 arms
H_2L^{2+}	2.04 - 2.12	qn	6	CH_2 ring
	2.15	s	9	SCH_3
	2.84	t	6	SCH_2
	3.10 - 3.19	m	18	NCH_2 ring + NCH_2 arms
H_3L^{3+}	2.15	s	9	SCH_3
	2.27 - 2.35	qn	6	CH_2 ring
	2.92	t	6	SCH_2
	3.46 - 3.54	m	18	NCH_2 ring + NCH_2 arms

s = singlet; t = triplet; m = multiplet; qn = quintet

Table S2. Chemical shift, multiplicity, relative integral, and ^{1}H resonance assignments for TRI4S. Data were taken from **Fig. S3**.

Species	δ [ppm]	Multiplicity	Relative Integral	Assignation
L	1.65	m	2	CH_2 ring
	2.14	s	12	SCH_3
	2.61	m	4	NCH_2 ring
	2.64 - 2.80	m	24	SCH_2 + NCH_2 ring + NCH_2 arms
HL^+	1.89	m	2	CH_2 ring
	2.16	s	6	SCH_3
	2.17	s	6	SCH_3
	2.72 - 2.89	m	24	SCH_2 + NCH_2 ring + NCH_2 arms
	2.98 - 3.03	m	8	
H_2L^{2+}	2.00	m	2	CH_2 ring
	2.18	s	6	SCH_3
	2.19	s	6	SCH_3
	2.86	t	8	SCH_2
	3.05 - 3.26	m	24	NCH_2 ring + NCH_2 arms
H_3L^{3+}	2.16	s	6	SCH_3
	2.17	s	6	SCH_3
	2.25	m	2	CH_2 ring
	2.87	t	4	SCH_2
	2.93	t	4	SCH_2
	3.21	t	4	NCH_2 arms
	3.34	s	4	NCH_2 ring (^1H_b)
	3.47 - 3.53	m	12	NCH_2 arms + NCH_2 ring (^1H_a + ^1H_c)
	3.67	t	4	NCH_2 ring (^1H_a)

s = singlet; t = triplet; m = multiplet

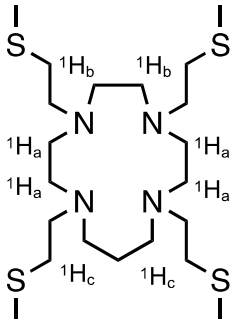

Table S3. Chemical shift, multiplicity, relative integral, and ^{1}H resonance assignments for TE4S. Data were taken from **Fig. S4.**

Species	δ [ppm]	Multiplicity	Relative integral	Assignation
L	1.70	m	4	CH_2 ring
	2.13	s	12	SCH_3
	2.55 - 2.81	m	4	SCH_2 + NCH_2 ring + NCH_2 arms
HL^+	2.00	m br	4	CH_2 ring
	2.16	s	12	SCH_3
	3.02	m	4	SCH_2 + NCH_2 ring + NCH_2 arms
H_2L^{2+}	2.00	m	4	CH_2 ring
	2.16	s	12	SCH_3
	2.83	t	8	SCH_2
	3.11	m	8	NCH_2 ring (^1H_b)
	3.03	m	8	NCH_2 arms
	3.17	s	8	NCH_2 ring (^1H_a)
H_3L^{3+}	2.16	s	12	SCH_3
	2.16	m	4	CH_2 ring
	2.95	t	8	SCH_2
	3.58	m	8	NCH_2 ring (^1H_b)
	3.53	m	8	NCH_2 arms
	3.84	s	8	NCH_2 ring (^1H_a)

s = singlet; t = triplet; m = multiplet; br = broad

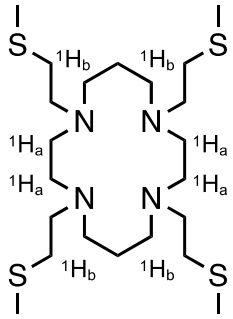

Table S4. Approximate timing required to reach the equilibrium during the reaction between Cu^{2+} and TACD3S, TRI4S and TE4S (C_L = $C_{Cu^{2+}}$ = 1·10^{-4} M) at room temperature at various pH. Data were taken from **Fig. S14** - **S15**.

pH	Equilibration time			
	TACD3S	**TRI4S**	**TE4S**	**DO4S** [c]
2.0	[a]	2 d	[a]	~ 10 d
3.7	[a]	40 min	20 min	~ 20 h
7.5	< 10 sec [b]	< 10 sec	< 10 sec	< 10 sec

[a] No Cu^{2+} complex formation.
[b] Not quantitative.
[c] From ref. [1].

Table S5. pCu^{2+} values (C_L = 1·10^{-5} M, $C_{Cu^{2+}}$ = 1·10^{-6} M, pH 7.4) for the cupric complexes formed by sulfur-bearing cyclen derivatives (DO3S, DO3SAm and DO2A2S) and selected state-of-the-art $^{64/67}Cu^{2+}$ ligands (DOTA, NOTA and TETA).[1]

Ligand	pCu^{2+}
DO3S	17.5
DO3SAm	17.2
DO2A2S	19.4
DOTA	17.4
NOTA	18.2
TETA	16.2

Table S6. UV-Vis spectroscopic parameters for the Cu^{2+} complexes with TRI4S and TE4S. Data for Cu^{2+}-DO4S are reported for comparison purposes.

Complex	**LMCT** [a]		***d-d*** [b]	
	λ_{max} [nm]	**ε [L/cm·mol]**	**λ [nm]**	**ε [L/cm·mol]**
Cu^{2+}-TRI4S	313	(4.6 ± 0.4)·10^3	598	6.9·10^2
Cu^{2+}-TE4S	313	(4.5 ± 0.5)·10^3	626	4.1·10^2
Cu^{2+}-DO4S [c]	309	(3.6 ± 0.9)·10^3	593	5.3·10^2

[a] Obtained from the UV-Vis data fitting.
[b] Estimated from the spectra.
[c] Taken from ref. [1].

Table S7. Percentage of Cu^{2+} intact complexes [%] of TRI4S and TE4S in presence of Zn^{2+} excess at t = 5 days after the metal competitor addition (see **Fig. S21**).

	$n(Zn^{2+})/n(CuL^{2+})$	50	100	200	500	1000
Intact Complex [%]	Cu^{2+}-TRI4S	92	93	89	95	99
	Cu^{2+}-TE4S	98	99	97	96	93

Table S8. Percentage of Cu^{2+} intact complexes [%] of TRI4S and TE4S in presence of Ni^{2+} excess at t = 5 days after the metal competitor addition (see **Fig. S22**).

	$n(Ni^{2+})/n(CuL^{2+})$	50	100	150	200	250
Intact Complex [%]	Cu^{2+}-TRI4S	96	93	97	93	94
	Cu^{2+}-TE4S	97	92	92	91	92

Table S9. $^{d}k_{obs}$ values for the Cu^{2+} complexes of DO4S, DO2A2S, TRI4S and TE4S in HCl at different concentrations.

	$^{d}k_{obs}\cdot10^{5}$ [s^{-1}]			
[HCl] [M]	DO4S	DO2A2S	TRI4S	TE4S
0.1	4.5 ± 0.8	1.08 ± 0.02	22.9 ± 0.3	1100 ± 100
0.2	9.8 ± 0.2	2.20 ± 0.03	300 ± 9	1300 ± 100
0.4	19.8 ± 0.3	4.78 ± 0.05	802 ± 59	1520 ± 50
0.6	33 ± 3	6.5 ± 0.1	1831 ± 72	−
0.8	45 ± 1	8.2 ± 0.1	2850 ± 110	−
1.0	59 ± 6	10.4 ± 0.3	3400 ± 260	−

Table S10. Acid decomplexation half-life ($t_{1/2}$) of the Cu^{2+} complexes with first- and second-generation sulfur-bearing macrocycles and corresponding second order dissociation rate constants (^{d}k, $^{d}k_2$) determined by fitting the experimental data with the equation $^{d}k_{obs} = {}^{d}k[H^+]$ (for DO4S, DO2A2S, and TE4S) or $^{d}k_{obs} = {}^{d}k\,[H^+] + {}^{d}k_2\,[H^+]^2$ (for TRI4S).

[HCl] [M]	Half-life ($t_{1/2}$)			
	DO4S [min]	DO2A2S [h]	TRI4S [min]	TE4S [min]
0.1	254	17.8	50.4	1.0
0.2	118	8.8	3.8	0.9
0.4	58.3	4.0	1.4	0.7
0.6	35.3	2.9	0.6	
0.8	25.5	2.3	0.4	< 30 sec
1.0	19.4	1.8	0.3	
^{d}k [M^{-1} s^{-1}]	$(5.7 \pm 0.1)\cdot10^{-4}$	$(1.04 \pm 0.02)\cdot10^{-4}$	$(1.7 \pm 0.6)\cdot10^{-2}$	~ 10^{-2}
$^{d}k_2$ [M^{-1} s^{-1}]	-	-	$(1.9 \pm 0.7)\cdot10^{-2}$	

Table S11. Chemical shift, multiplicity, relative integral, and ^{1}H resonance assignments for the Cu^{+} complexes with TRI4S and TE4S. Data were taken from **Fig. 6.**

Complex	δ [ppm]	Multiplicity	Relative integral	Assignation
Cu^{+}-TRI4S	2.00	s	1	$CH_{2,ax/eq}$
	2.31	s	1	$CH_{2,ax/eq}$
	2.50	s	6	SCH_3
	2.55	s	6	SCH_3
	2.96 - 3.30	m	32	SCH_2 + NCH_2 arms + NCH_2 ring
Cu^{+}-TE4S	1.93	s br	4	CH_2
	2.29	s	12	SCH_3
	2.63 - 3.10	m br	32	SCH_2 + NCH_2 arms + NCH_2 ring

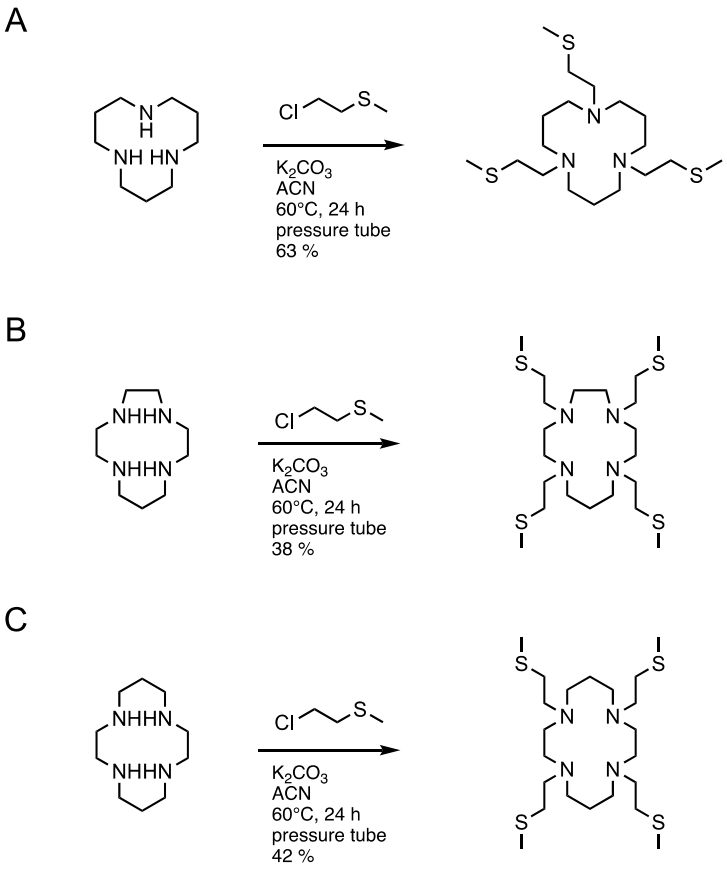

Scheme S1. Synthesis of (A) TACD3S, (B) TRI4S and (C) TE4S.

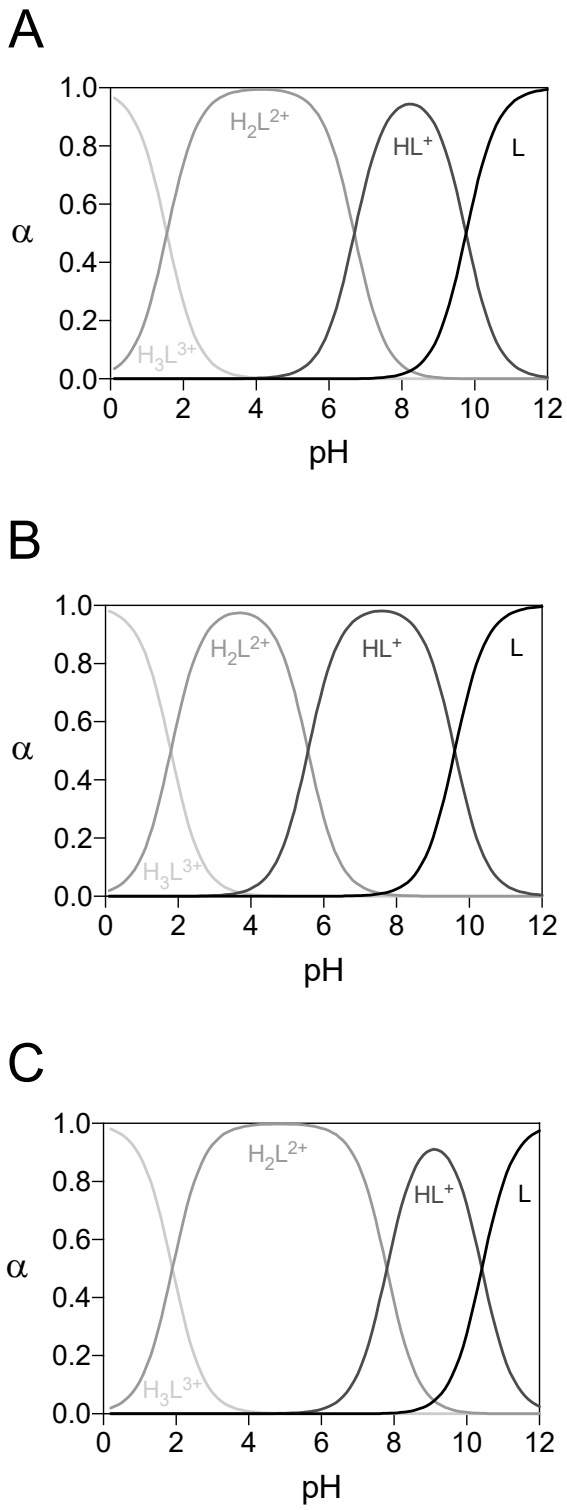

Fig. S1. Speciation diagram for (A) TACD3S, (B) TRI4S and (C) TE4S calculated using the protonation constants of **Table 1**.

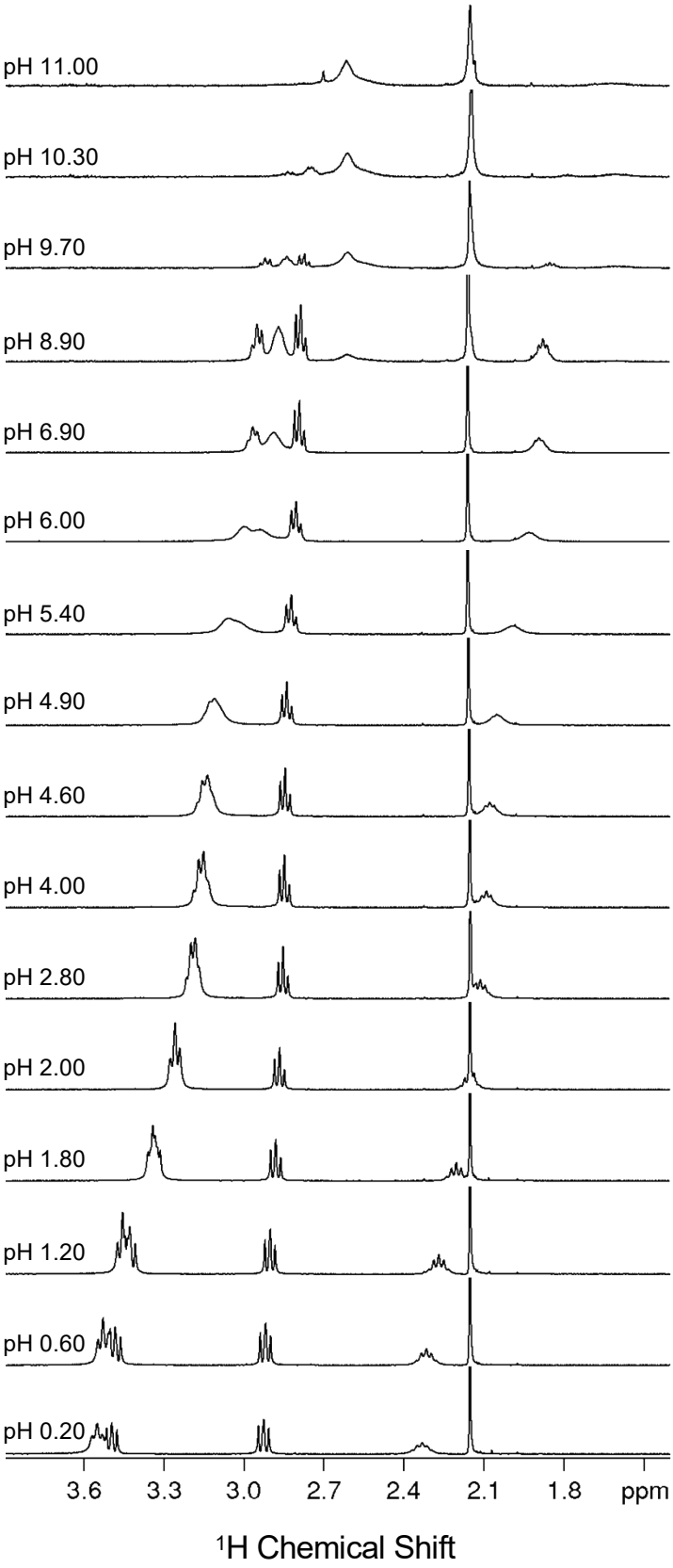

Fig. S2. ^{1}H NMR spectra of TACD3S (400 MHz, 25 °C, H_2O + 10% D_2O, C_{TACD3S} = $9.8 \cdot 10^{-4}$ M) at various pH values.

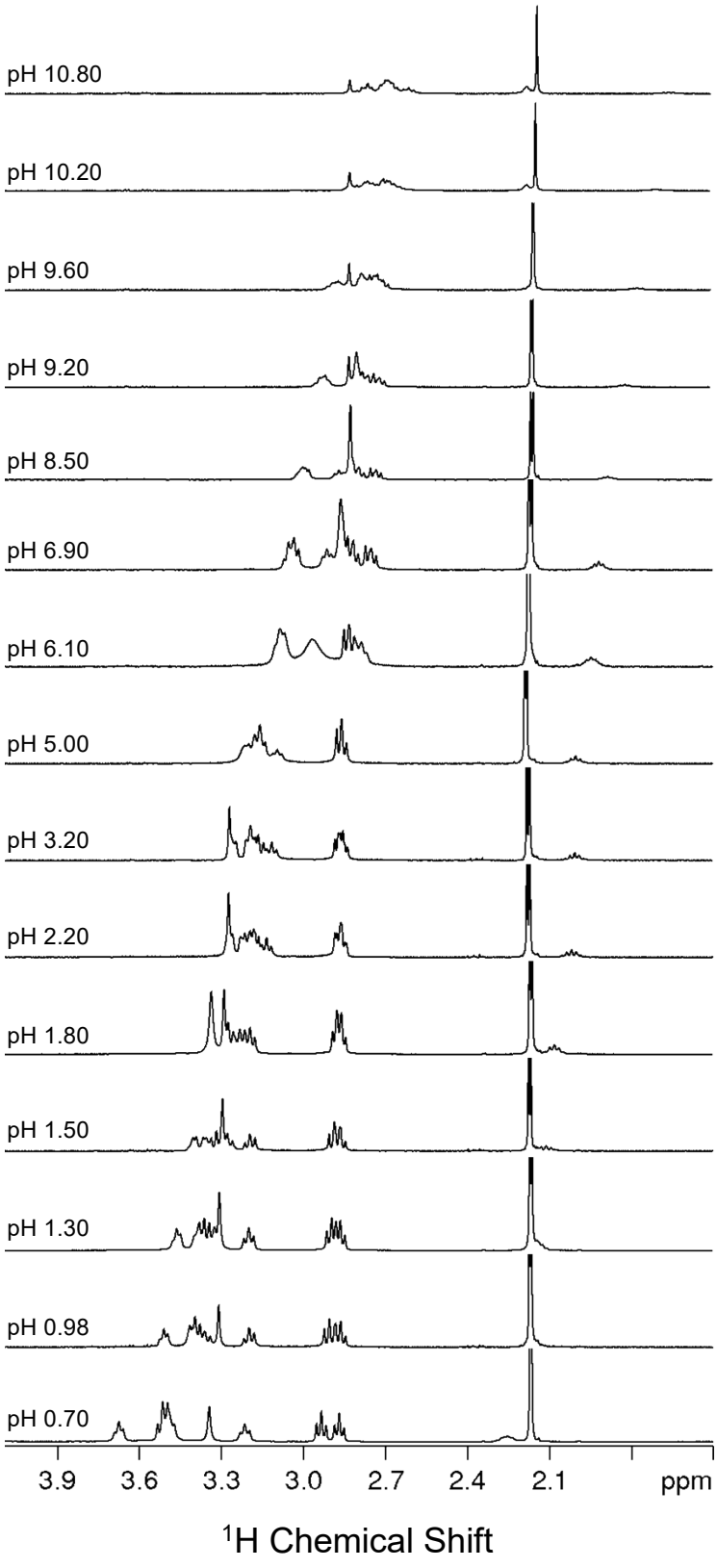

Fig. S3. ^{1}H NMR spectra of TRI4S (400 MHz, 25 °C, H_2O + 10% D_2O, C_{TRI4S} = 9.1·10^{-4} M) at various pH values.

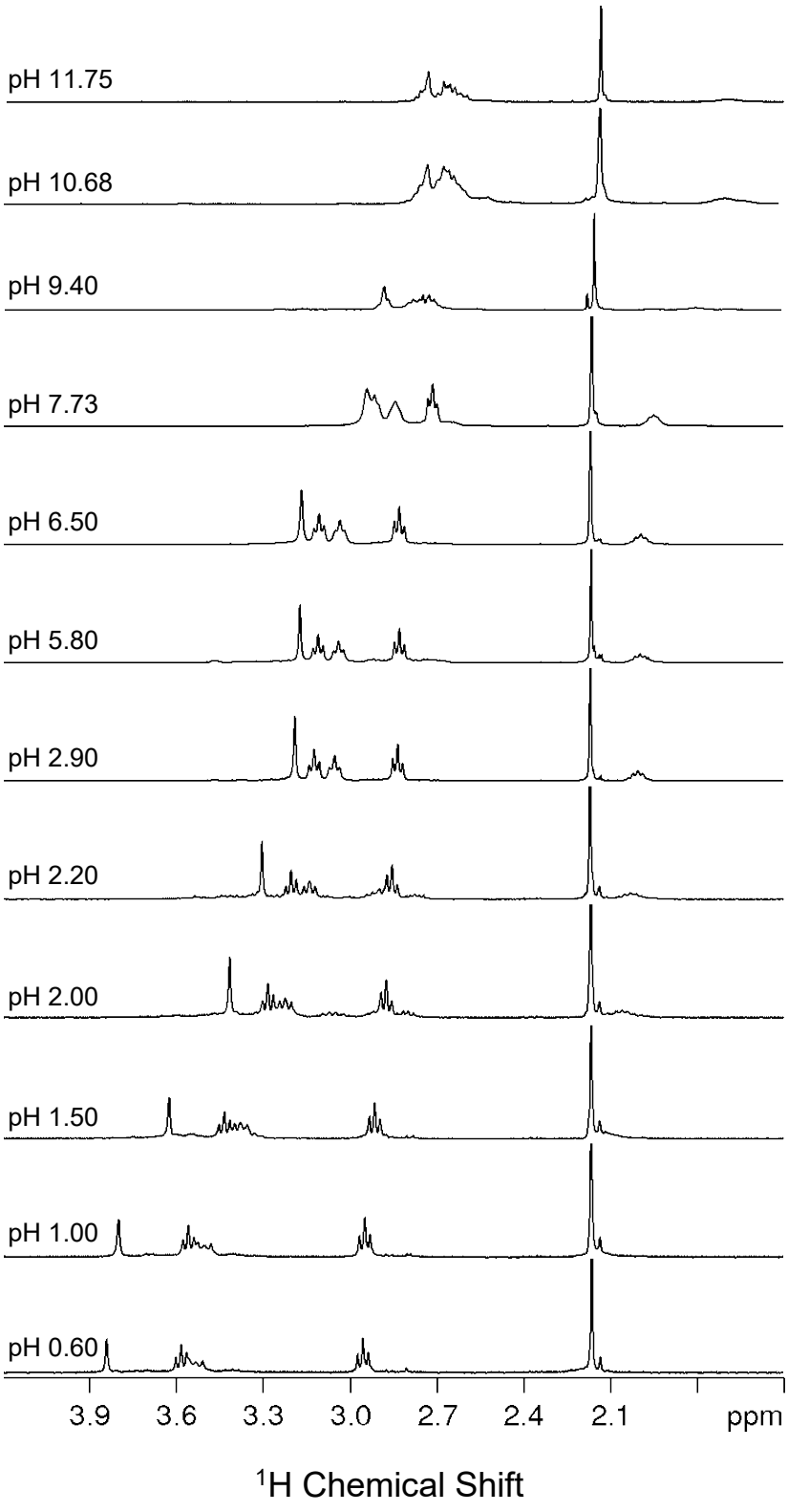

Fig. S4. ^{1}H NMR spectra of TE4S (400 MHz, 25 °C, H_2O + 10% D_2O, C_{TE4S} = 9.7·10^{-4} M) at various pH values.

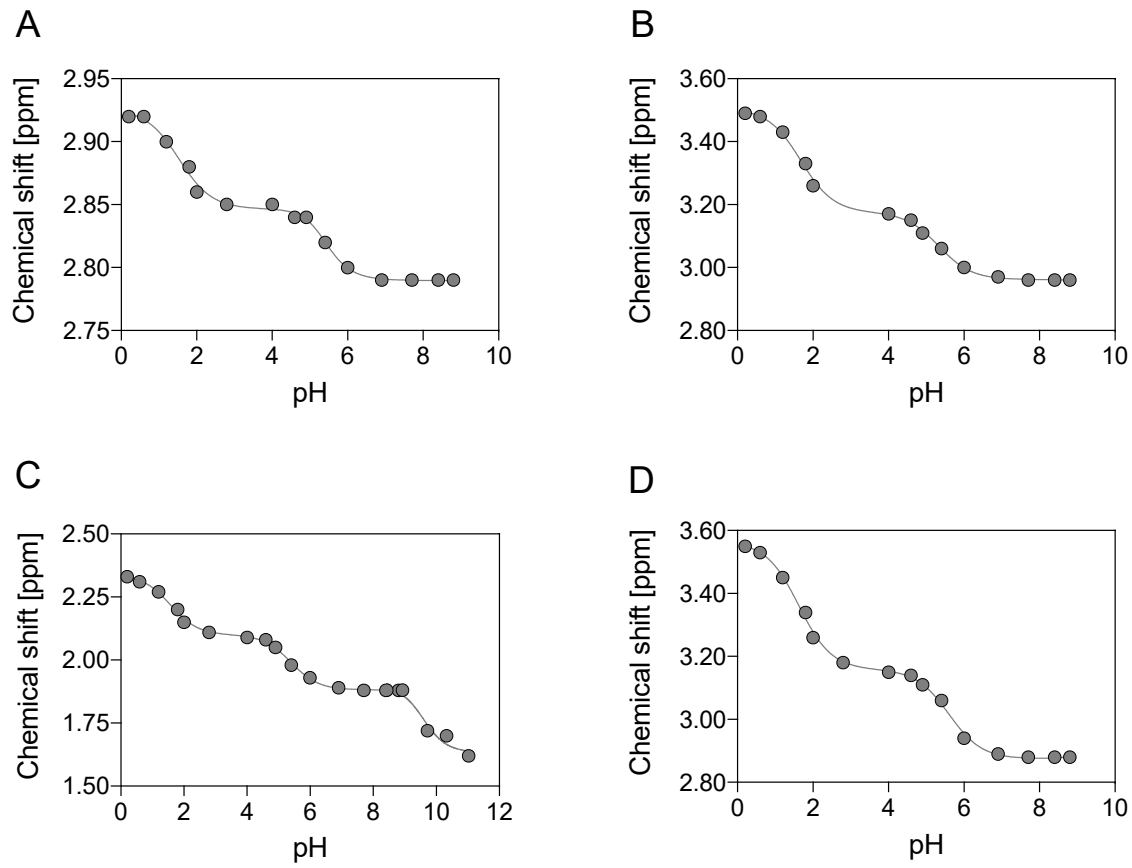

Fig. S5. Representative ^{1}H-NMR titration curves and corresponding fitting lines of TACD3S (data points were taken from **Fig. S2**) for (A) SCH_2 arms protons, (B) NCH_2 arms protons, (C) CH_2 ring protons and (D) NCH_2 ring protons.

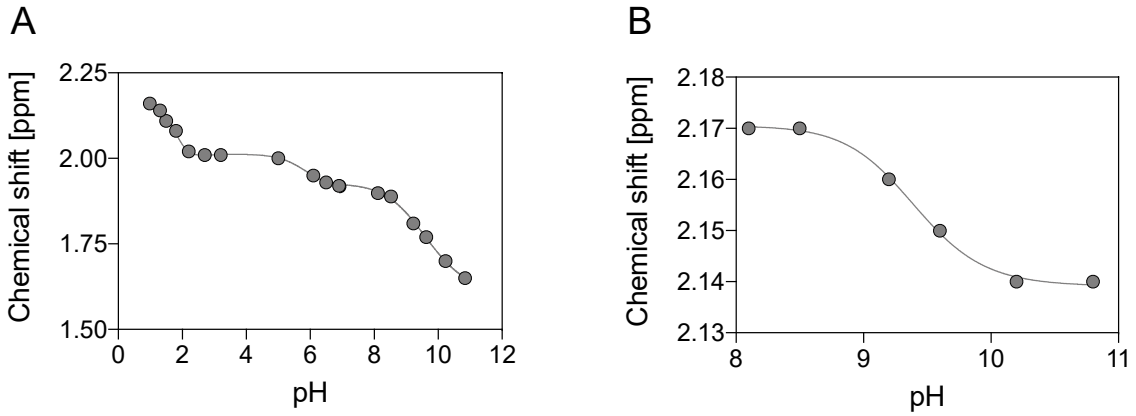

Fig. S6. Representative ^{1}H-NMR titration curves and corresponding fitting lines of TRI4S (data points were taken from **Fig. S3**) for (A) CH_2 ring protons and (B) SCH_3 arms protons.

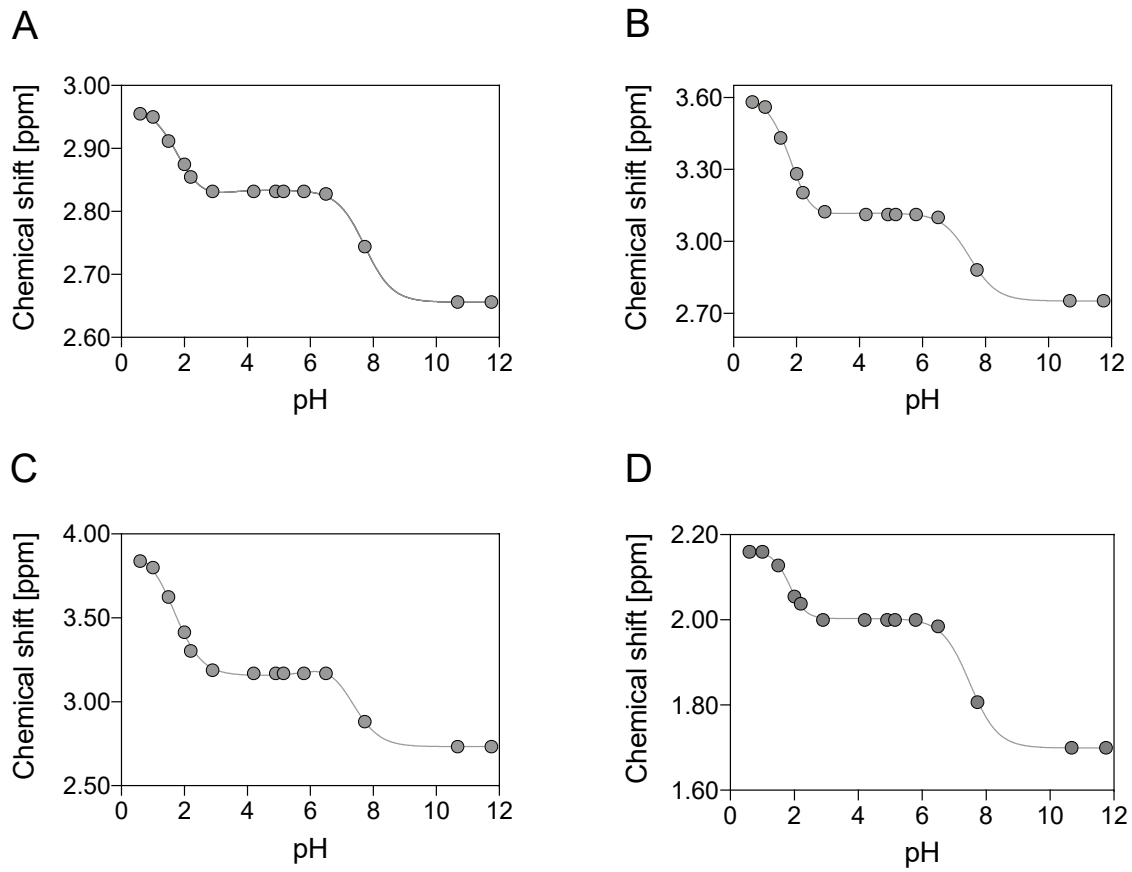

Fig. S7. Representative ^{1}H-NMR titration curves and corresponding fitting lines of TE4S (data points were taken from **Fig. S4**) for (A) SCH_2 arms protons, (B) NCH_2 arms protons, (C) NCH_2 ring protons and (D) CH_2 ring protons.

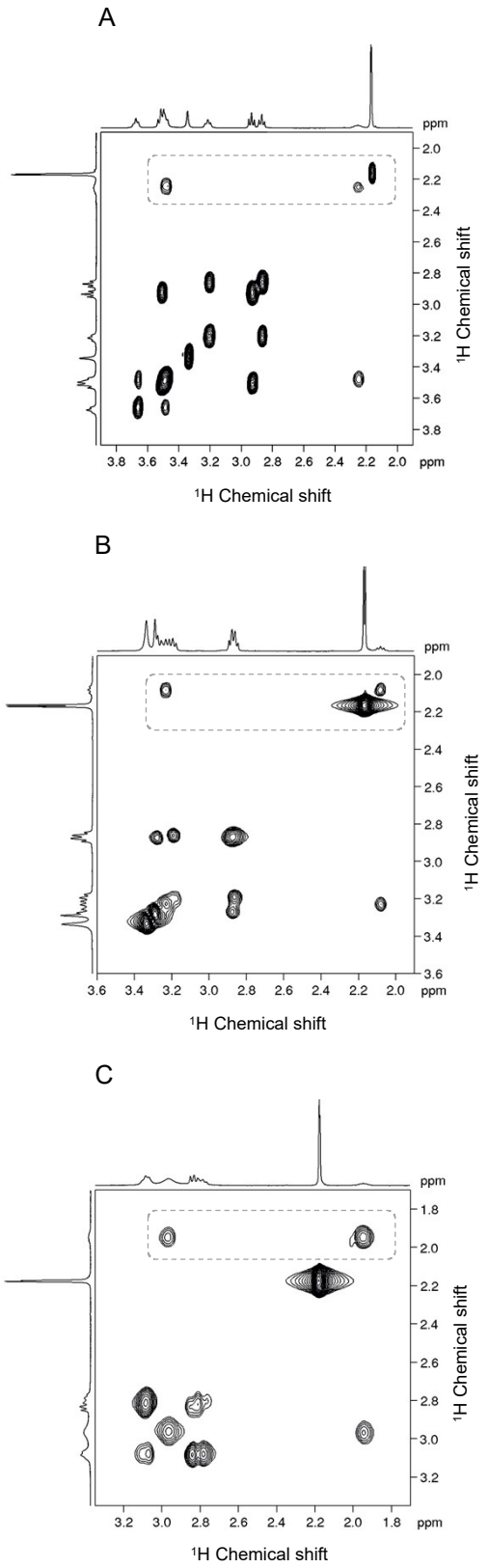

Fig. S8. TOCSY spectra of TRI4S at (A) pH 0.7, (B) pH 1.8 and (C) pH 6.1 (see also caption of **Fig. S3**). Intensity scale for ring CH_2 signal is different from those used for the others.

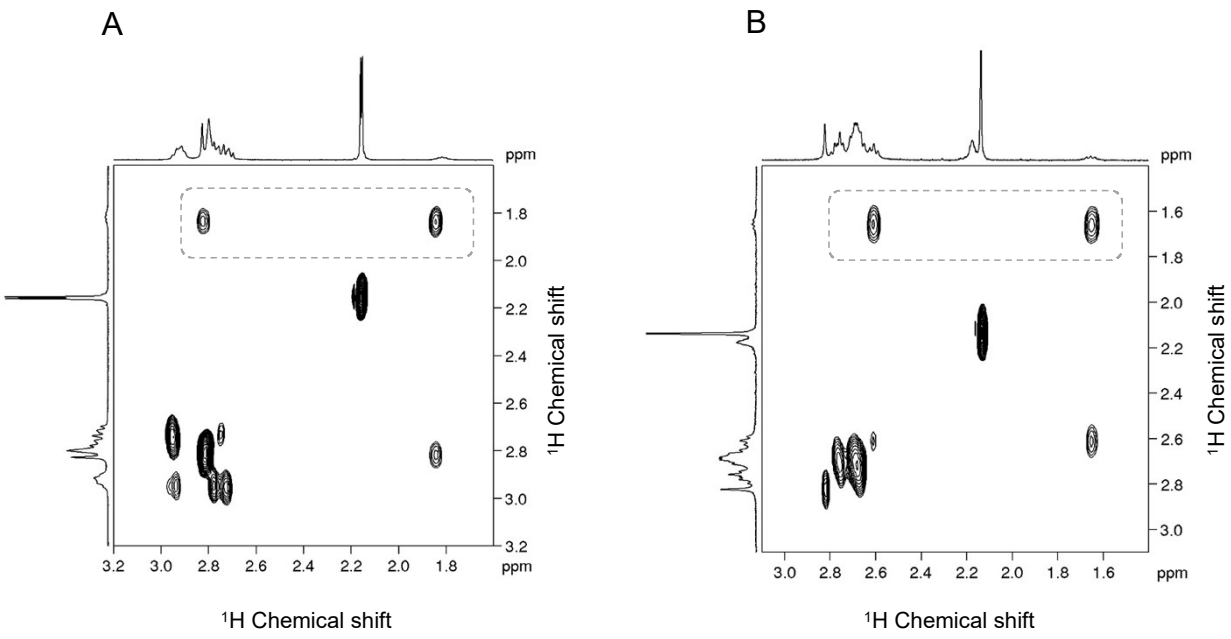

Fig. S9. TOCSY spectra of TRI4S at (A) pH 9.2 and (B) pH 10.8 (see also caption of **Fig. S3**). Intensity scale for ring CH_2 signal is different from those used for the others.

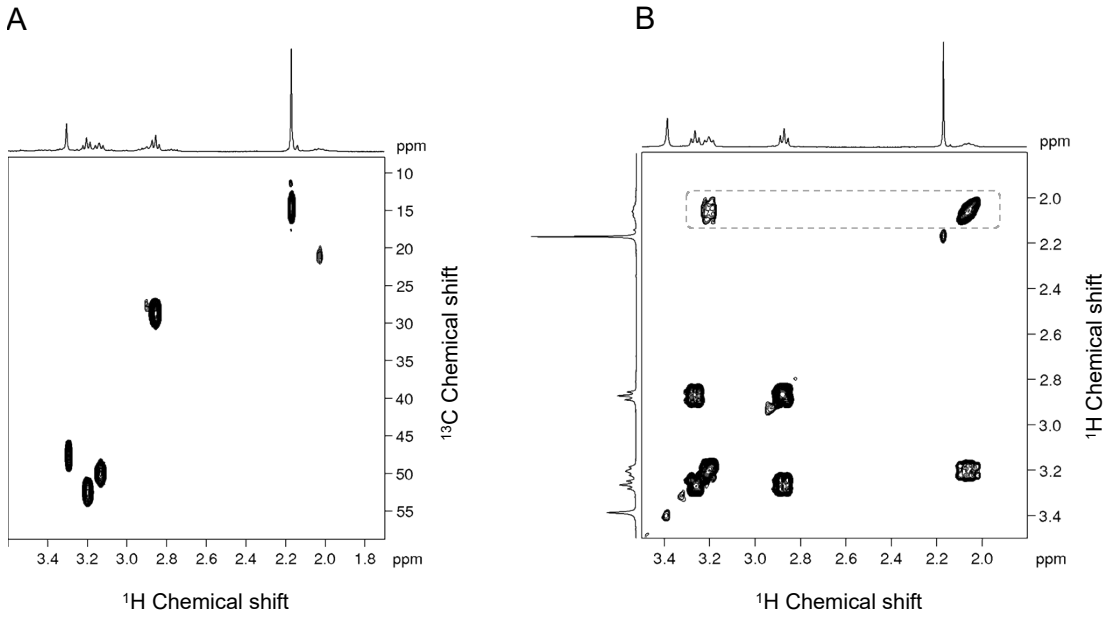

Fig. S10. (A) HSQC and (B) TOCSY spectra of TE4S at pH 1.7 (see also caption of **Fig. S4**). Intensity scale for ring CH_2 signal is different from those used for the others.

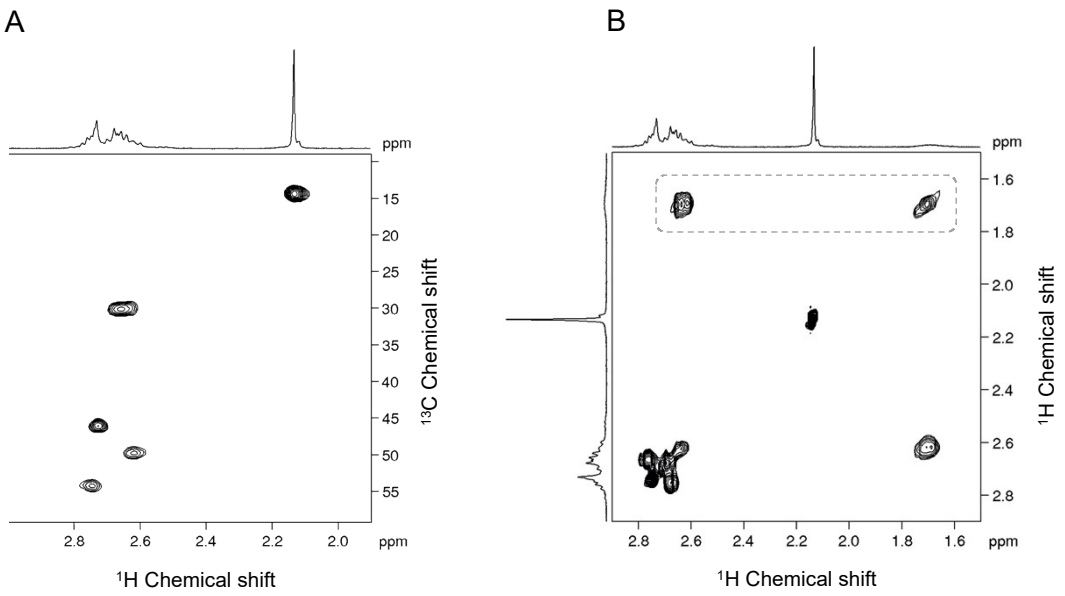

Fig. S11. (A) HSQC and (B) TOCSY spectra of TE4S at pH 12 (see also caption of **Fig. S4**). Intensity scale for ring CH_2 signal is different from those used for the others.

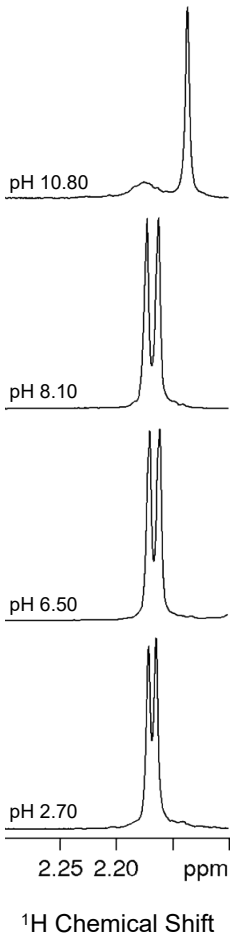

Fig. S12. Enlargement of ^{1}H NMR SCH_3 spectral region of TRI4S (see also caption of **Fig. S3**).

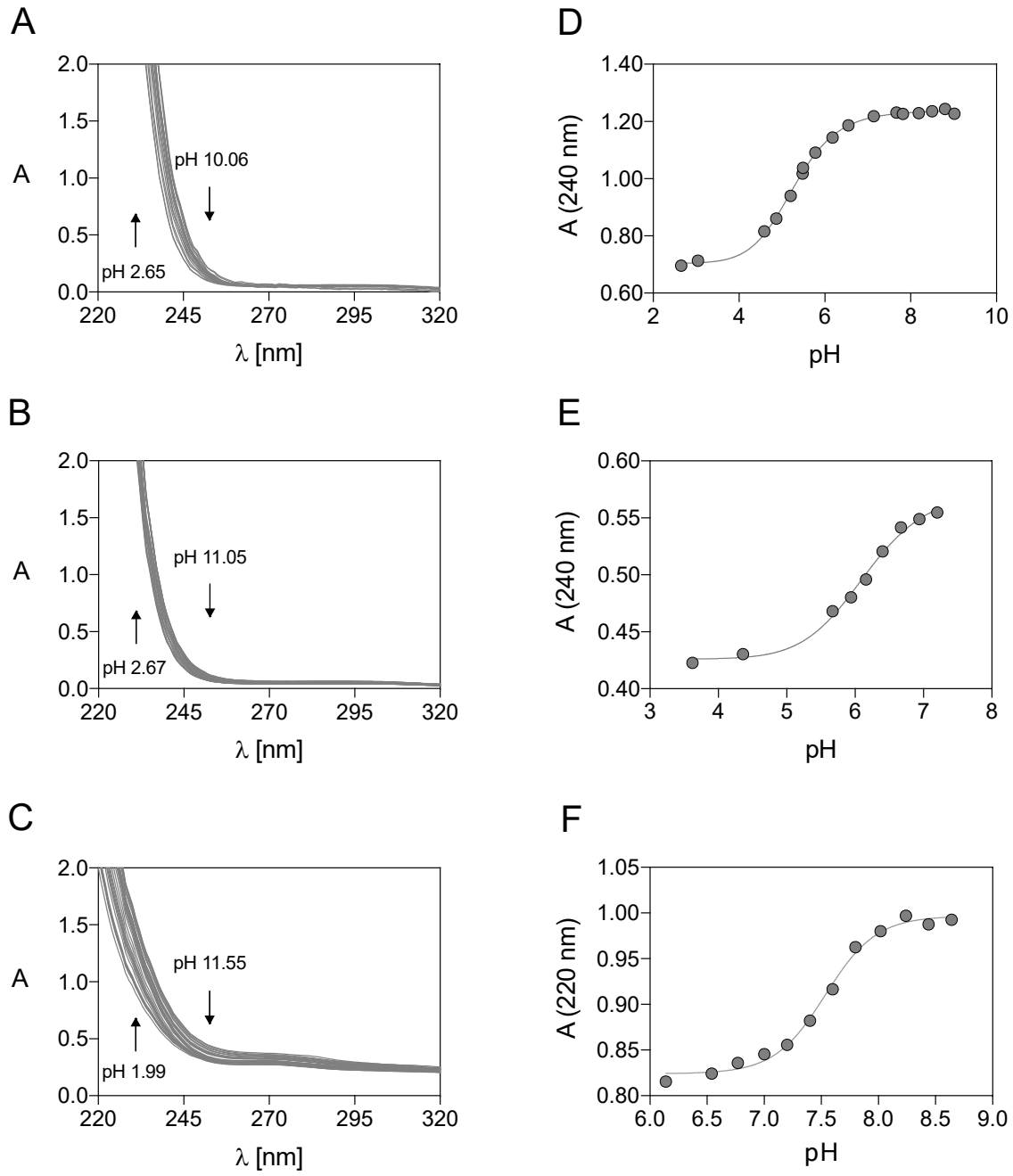

Fig. S13. UV-Vis spectra of solutions containing (A) TACD3S (C_{TACD3S} = 1.43·10^{-3} M, 2.65 ≤ pH ≤ 10.06), (B) TRI4S (C_{TRI4S} = 5.6·10^{-4} M, 2.67 ≤ pH ≤ 11.05) and (C) TE4S (C_{TE4S} = 5.4·10^{-4} M, 1.99 ≤ pH ≤ 11.55) and (D, E, F) corresponding experimental points and fitting line of absorbance *vs.* pH at selected λ.

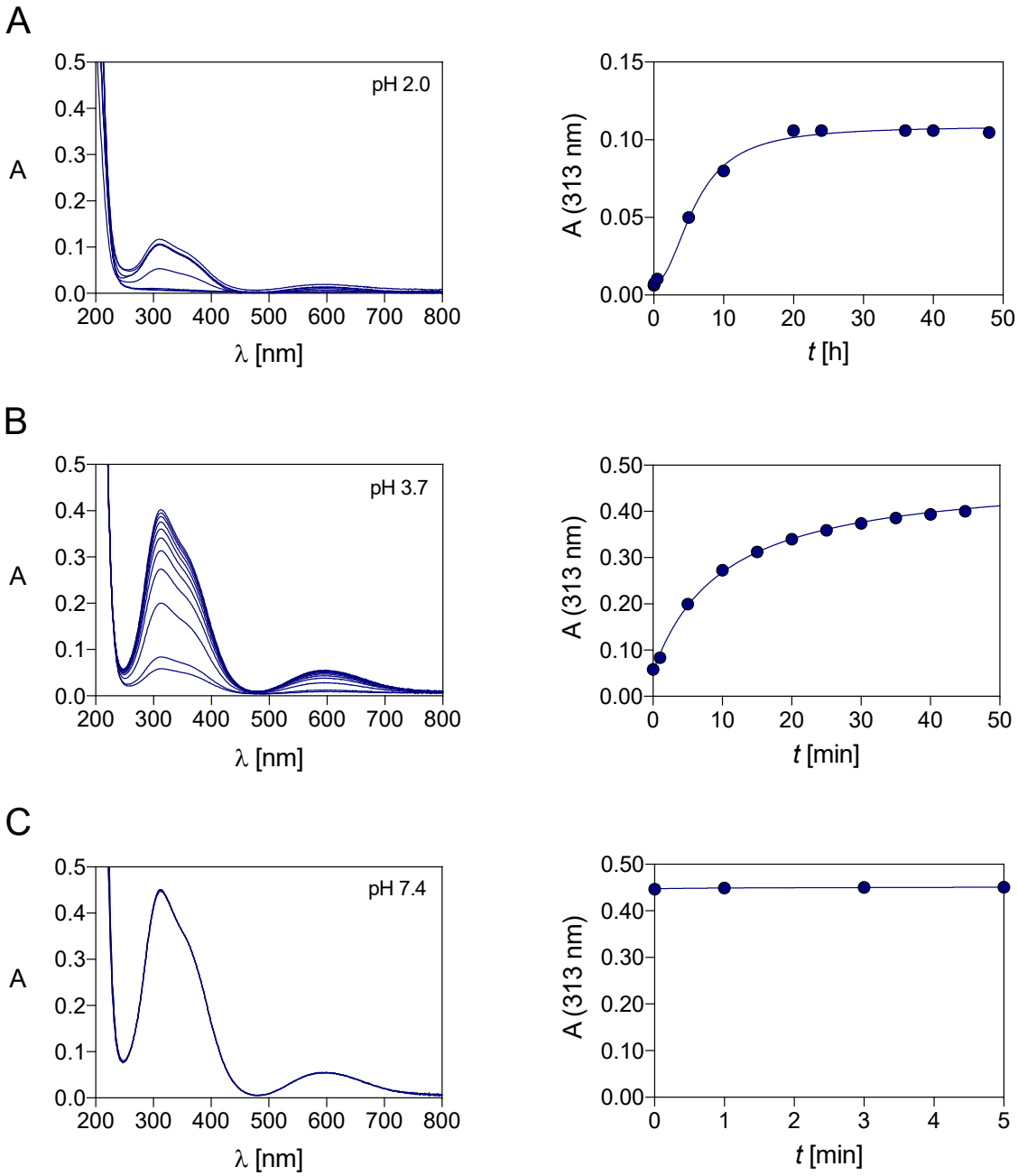

Fig. S14. UV-Vis spectra (left) and time course of the Cu^{2+} complexation (right) by TRI4S at (A) pH 2.0, (B) pH 3.7 and (C) pH 7.5 (C_{TRI4S} = $C_{Cu^{2+}}$ = $1.0 \cdot 10^{-4}$ M).

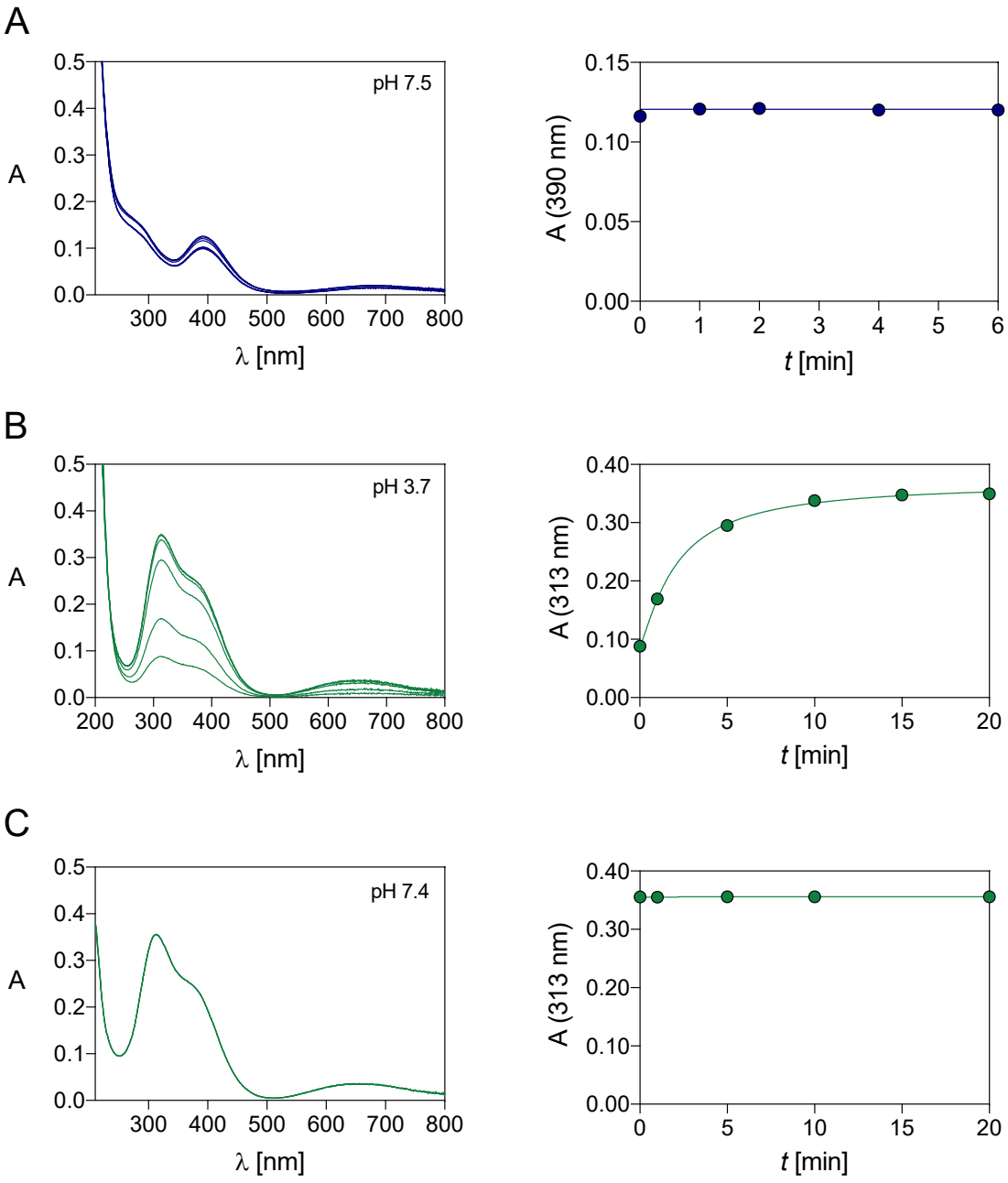

Fig. S15. UV-Vis spectra (left) and time course of the Cu^{2+} complexation (right) by (A) TACD3S at pH 7.5 (C_{TACD3S} = $C_{Cu^{2+}}$ = $1.0 \cdot 10^{-4}$ M) and Cu^{2+}-TE4S at (B) pH 3.7 and (C) pH 7.5 (C_{TE4S} = $C_{Cu^{2+}}$ = $7.0 \cdot 10^{-5}$ M).

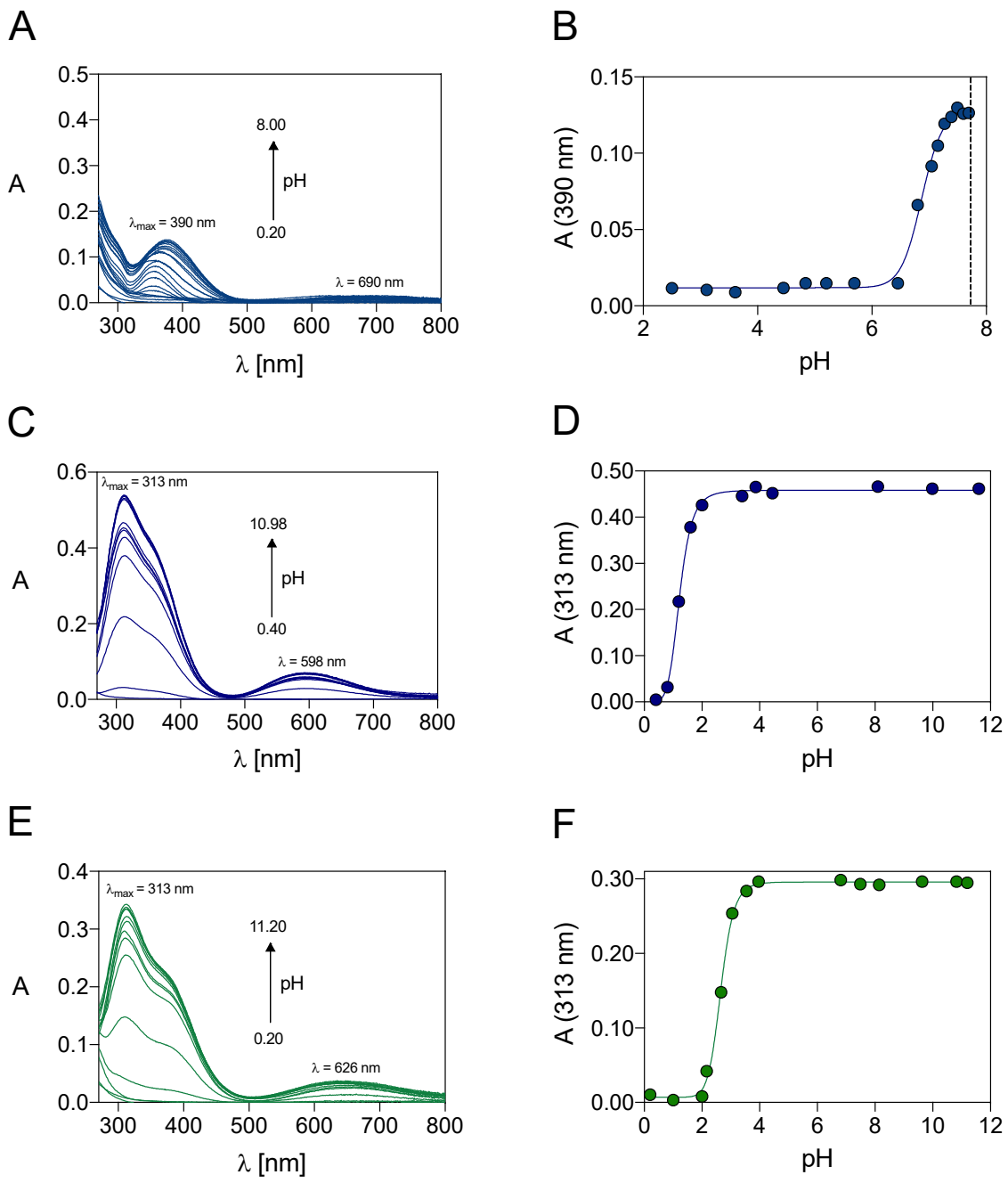

Fig. S16. Representative UV-Vis spectrophotometric titrations of the Cu^{2+} complexes with (A) TACD3S ($C_{Cu^{2+}}$ = C_{TACD3S} = $1.0 \cdot 10^{-4}$ M), (B) TRI4S ($C_{Cu^{2+}}$ = C_{TRI4S} = $1.0 \cdot 10^{-4}$ M) and (C) TE4S ($C_{Cu^{2+}}$ = C_{TE4S} = $7.0 \cdot 10^{-5}$ M) at I = 0.15 M NaCl and T = 25.0 °C.

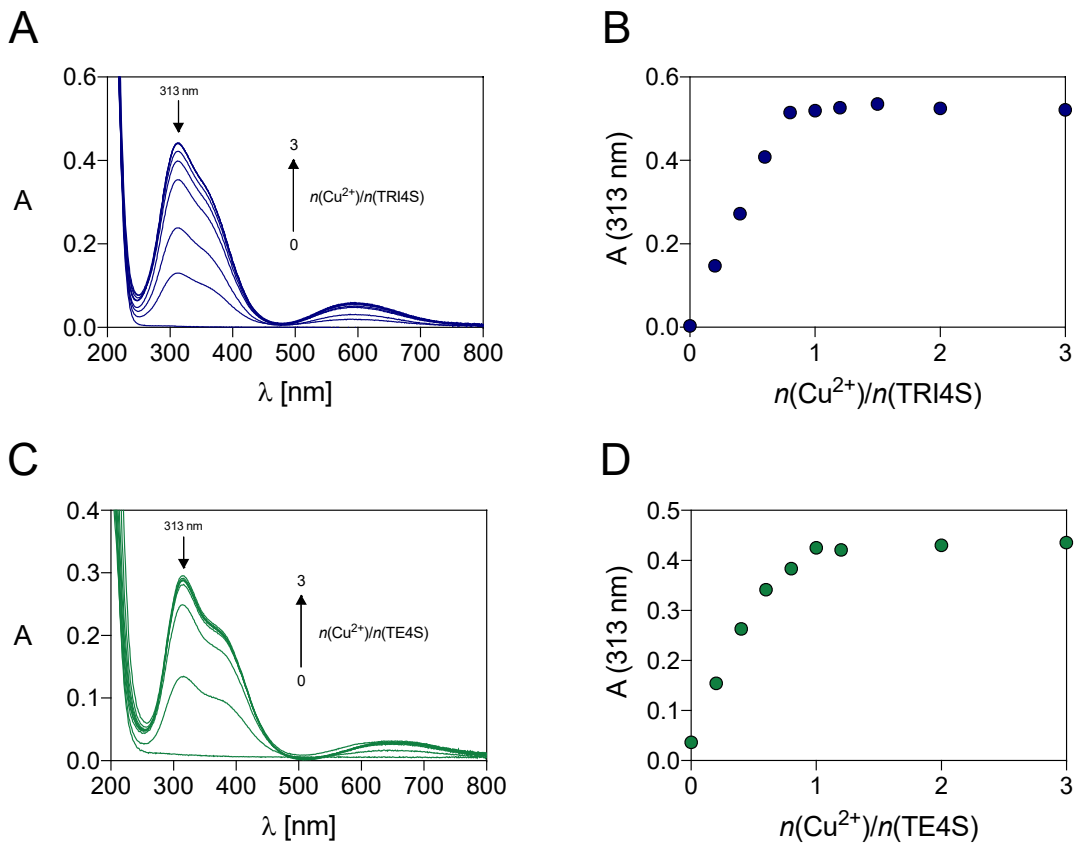

Fig. S17. UV-Vis spectrophotometric titrations at different metal-to-ligand molar ratio of the Cu^{2+} complexes with (A) TRI4S and (B) TE4S (C_L = 1.0·10^{-4} M) at pH 7.5 (no ionic strength control) and T = 25.0 °C.

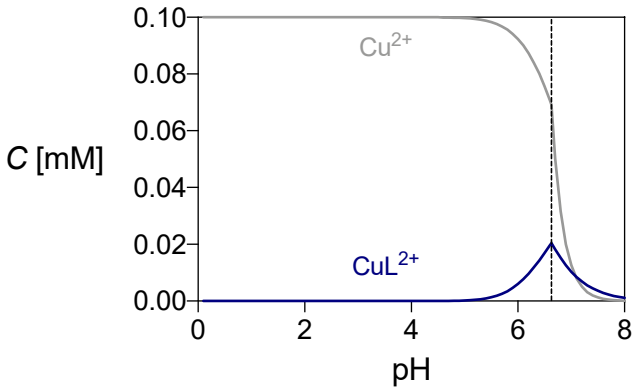

Fig. S18. Distribution diagram of Cu^{2+}-TACD3S. The plot was calculated from overall stability constants reported in **Tables 1** and **2** at $C_{Cu^{2+}}$ = C_{TACD3S} = 1.0·10^{-4} M. The dashed line represents the theoretical start of aged $Cu(OH)_2$ precipitation.

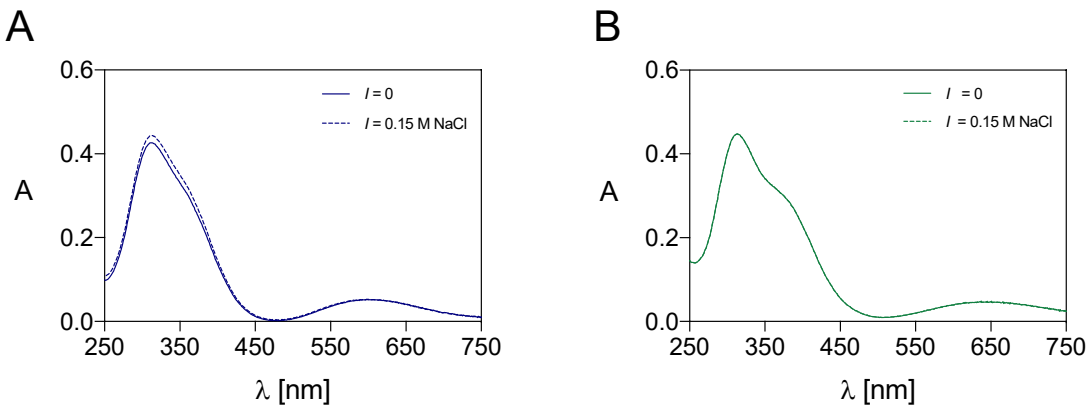

Fig. S19. Comparison of the UV-Vis spectra of the Cu^{2+} complexes with (A) TRI4S and (B) TE4S ($C_{Cu^{2+}}$ = C_L = $1.0 \cdot 10^{-4}$ M) at I = 0 M and I = 0.15 M NaCl (dotted line) and T = 25.0 °C.

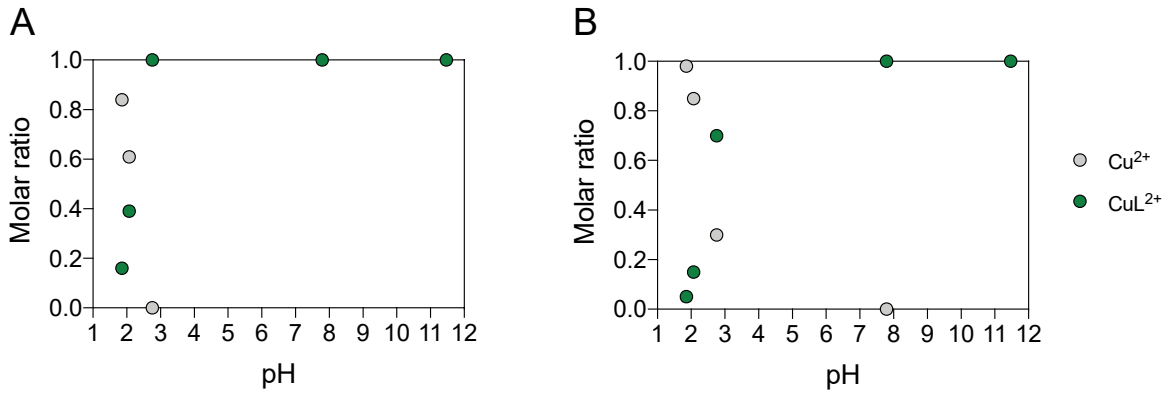

Fig. S20. Component ratios obtained from the simulation of Cu^{2+}-TE4S EPR spectra at (A) room temperature and (B) frozen solution at 77 K.

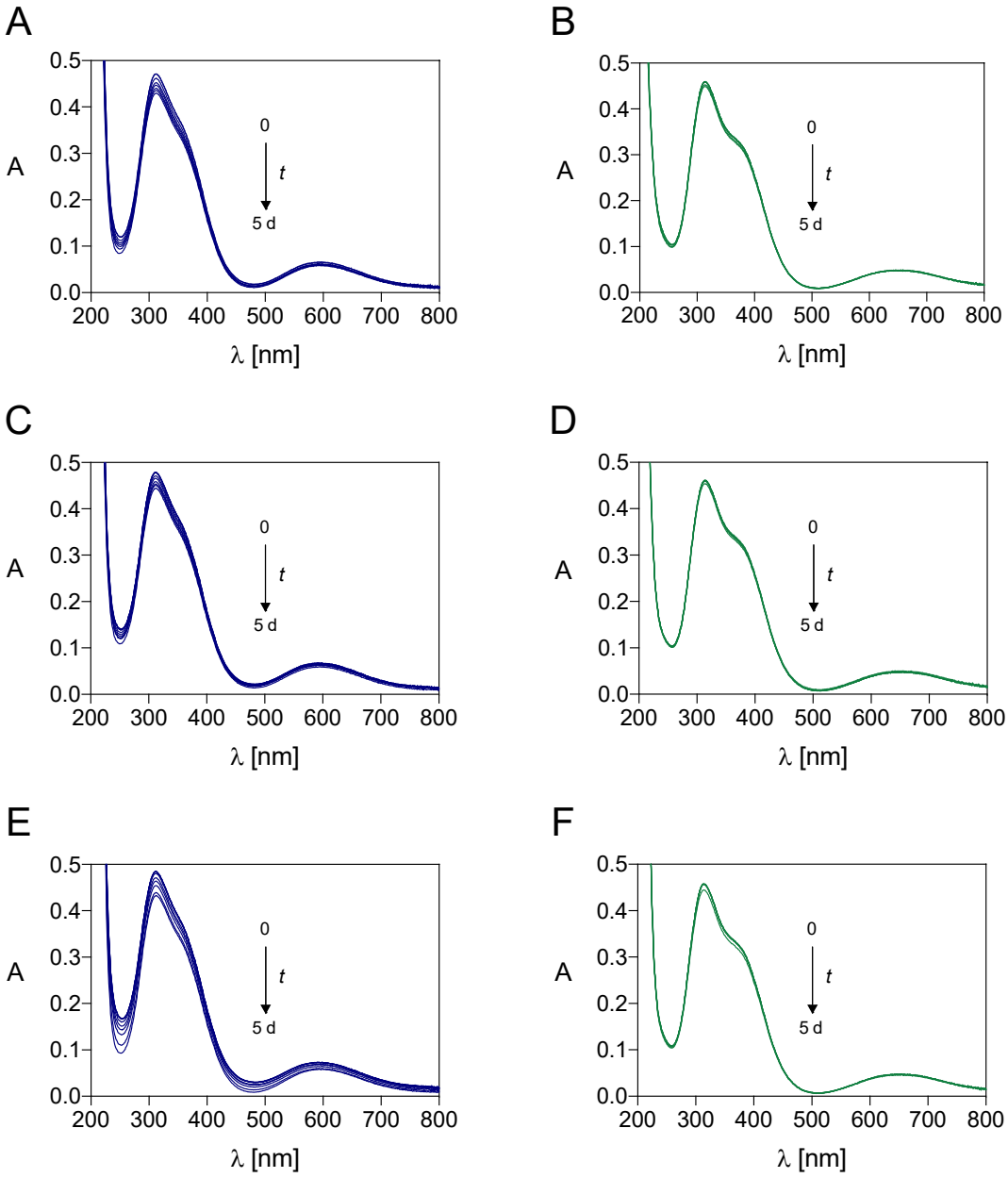

Fig. S21. UV-Vis spectra of the Zn^{2+} competition assays with (A, C, E) Cu^{2+}-TRI4S and (B, D, F) Cu^{2+}-TE4S at (A, B) n_{Zn}/n_{CuL} = 50, (C, D) n_{Zn}/n_{CuL} = 100; (E, F) n_{Zn}/n_{CuL} = 200 ($C_{Cu^{2+}} = C_L = 1.0 \cdot 10^{-4}$ M).

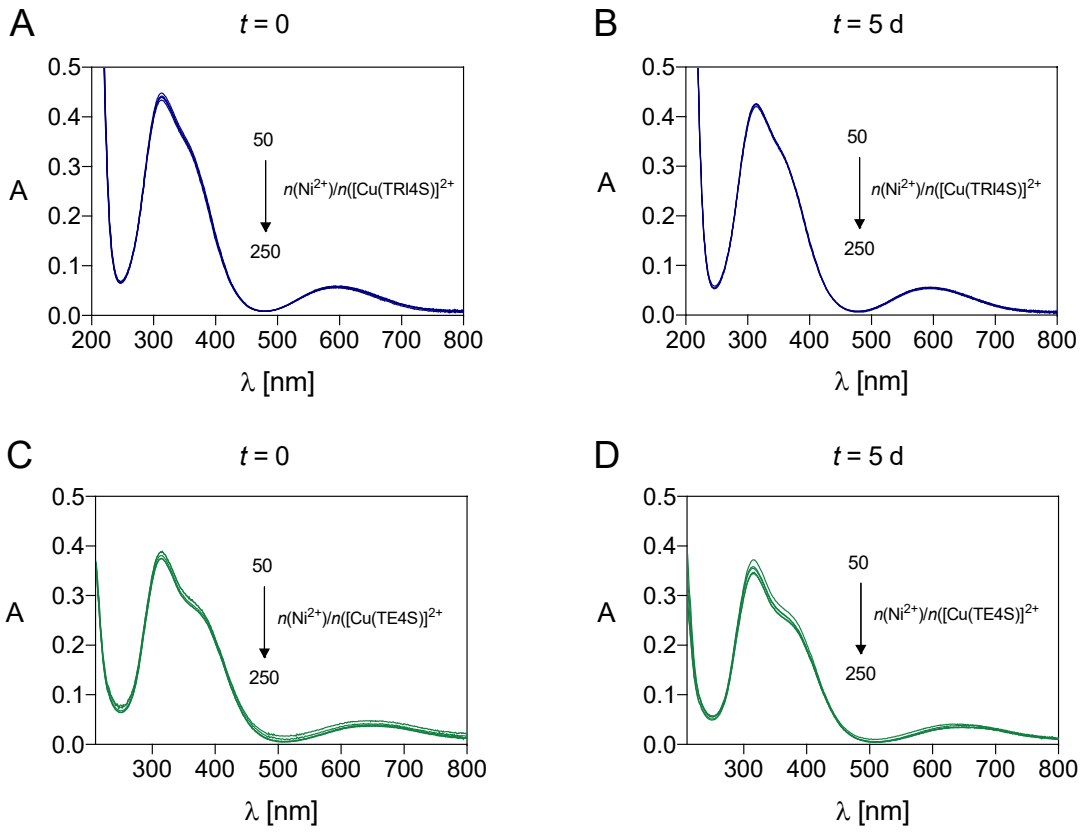

Fig. S22. UV-Vis spectra of the Ni^{2+} competition assays ($50 \leq n_{Ni}/n_{CuL} \leq 250$) with (A, B) Cu^{2+}-TRI4S and (C, D) Cu^{2+}-TE4S at $t = 0$ (after mixing) and $t = 5$ days.

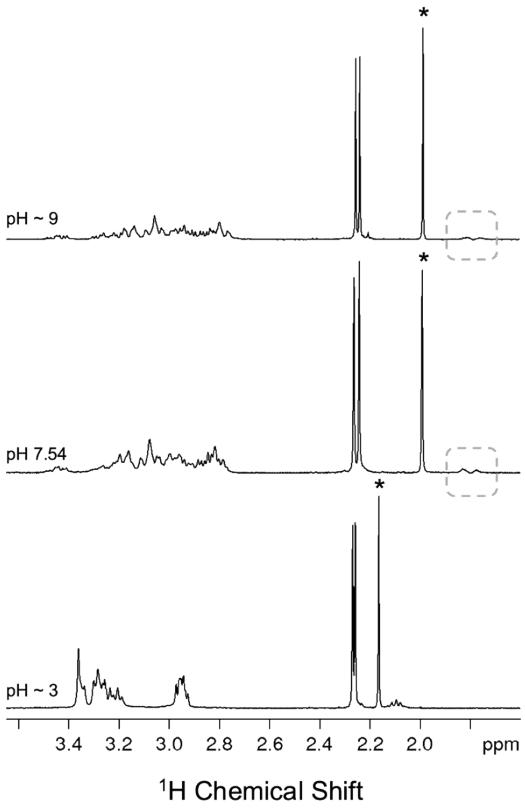

Fig. S23. Representative ^{1}H-NMR spectra (400 MHz, 25 °C, 10% D_2O + 90% H_2O) of the Zn^{2+}-TRI4S system at different pH values ($C_{Zn^{2+}} = C_L = 1.0 \cdot 10^{-3}$ M).
The spectra at pH ~ 3 correspond to those of the free ligand (see **Fig. S3**) while those at pH > 7 are indicative of the Zn^{2+}-complex formation which is likely ZnL^{2+}. The broad singlets at 1.78 ppm (1 ^{1}H) and 1.83 (1 ^{1}H) ppm (grey box) are related to the CH_2 protons of the macrocyclic ring (2 ^{1}H), which become non-equivalent after the metal coordination, while those at 2.24 ppm and 2.26 ppm (12 ^{1}H) are related to the SCH_3 protons of the side arms. The multiplet at 2.72 - 3.52 ppm contains all the other resonances (SCH_2 + NCH_2 protons of the pendants and the NCH_2 protons of the ring). The signals marked with an asterisk are related to acetate protons. If the complex is ZnL^{2+}, a logβ range between 14.5 and 15 can be estimated from the NMR data.

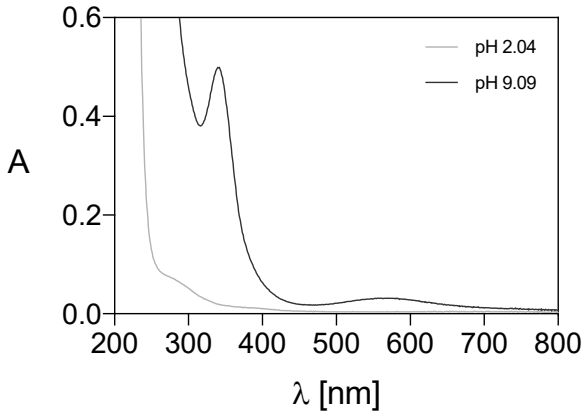

Fig. S24. Representative UV-Vis spectra of the Ni^{2+} complex with TRI4S ($C_{Ni^{2+}} = C_{TRI4S} = 1.0 \cdot 10^{-3}$ M) at different pH. The bands at λ = 366 nm and 566 nm at pH 9.09 have been attributed to the formation of a Ni^{2+}-complex. If this complex is NiL^{2+}, a logβ range between 13 and 16 can be estimated from the absorbance data.

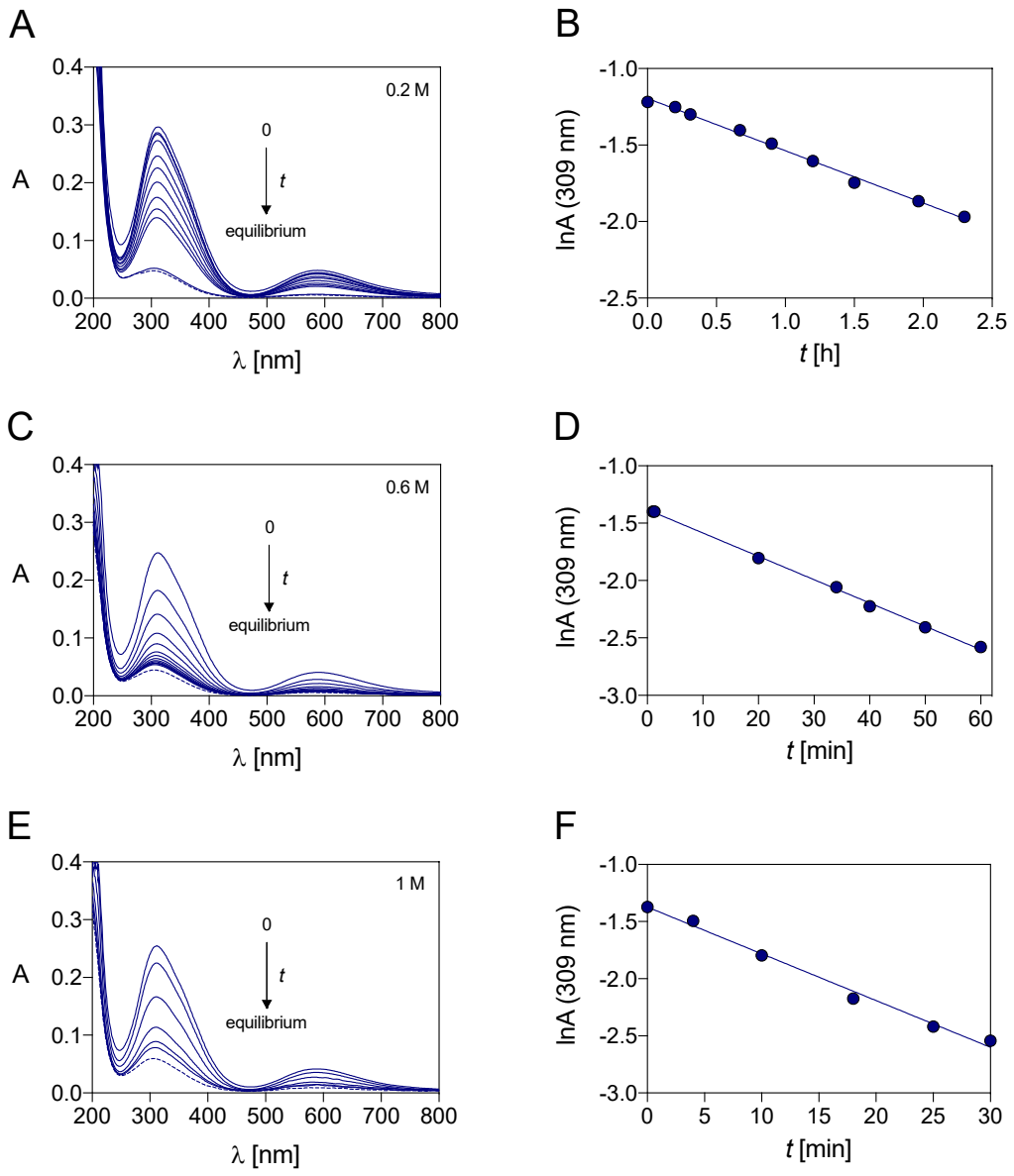

Fig. S25. (A, C, E) UV-Vis spectra variation during the acid-assisted decomplexation assays for Cu^{2+}-DO4S ($C_{Cu^{2+}} = C_{DO4S} = 1.0 \cdot 10^{-4}$ M) at the given (upper right) HCl concentrations (dotted lines correspond to equilibrium conditions). (B, D, F) ln*A vs. t* and corresponding fitting line.

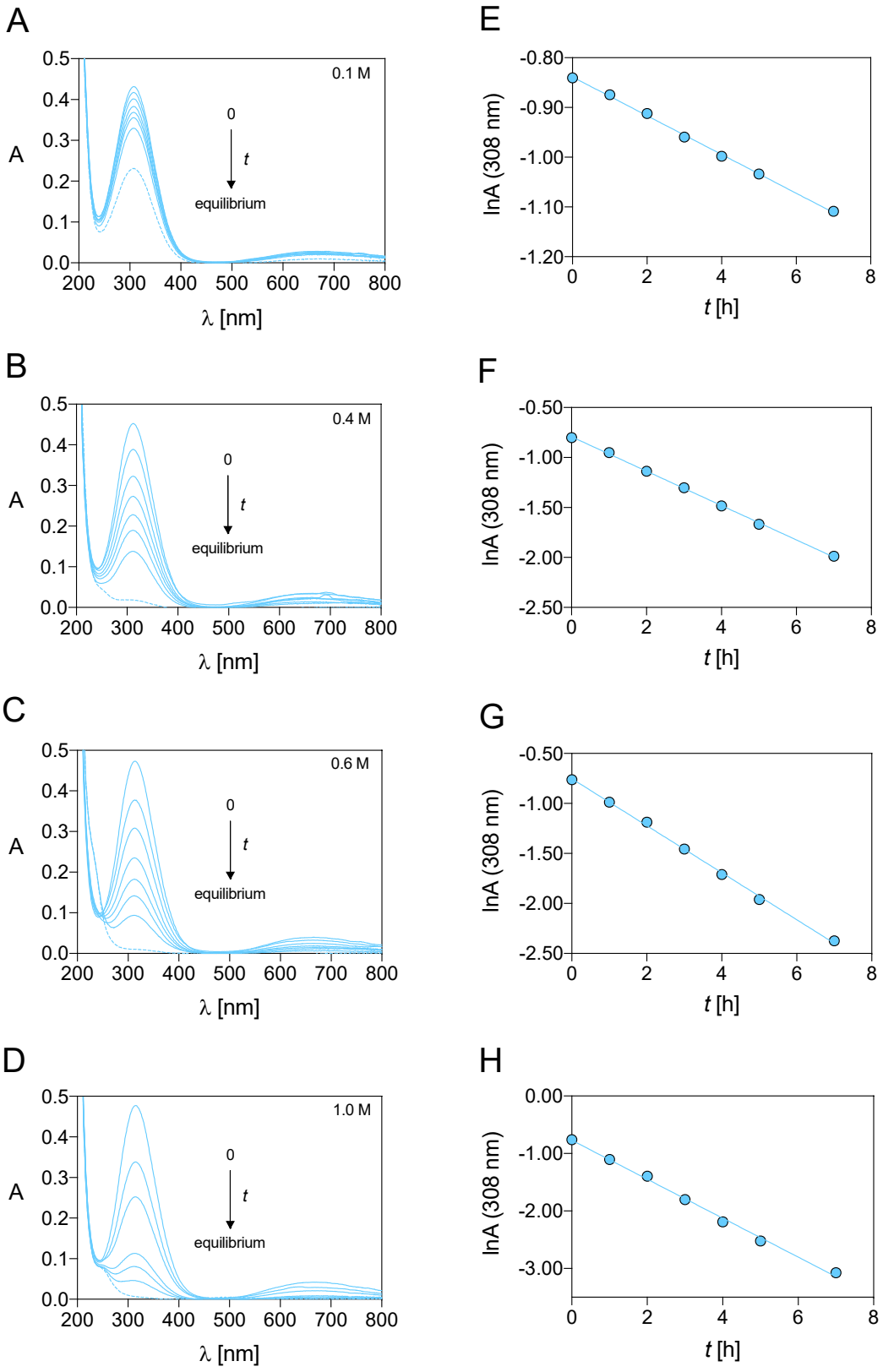

Fig. S26. (A, C, E, G) UV-Vis spectra variation during the acid-assisted decomplexation assays for Cu^{2+}-DO2A2S ($C_{Cu^{2+}}$ = C_{DO2A2S} = $1.0 \cdot 10^{-4}$ M) at the given (upper right) HCl concentrations (dotted lines correspond to equilibrium conditions). (B, D, F, H) ln*A vs. t* and corresponding fitting line.

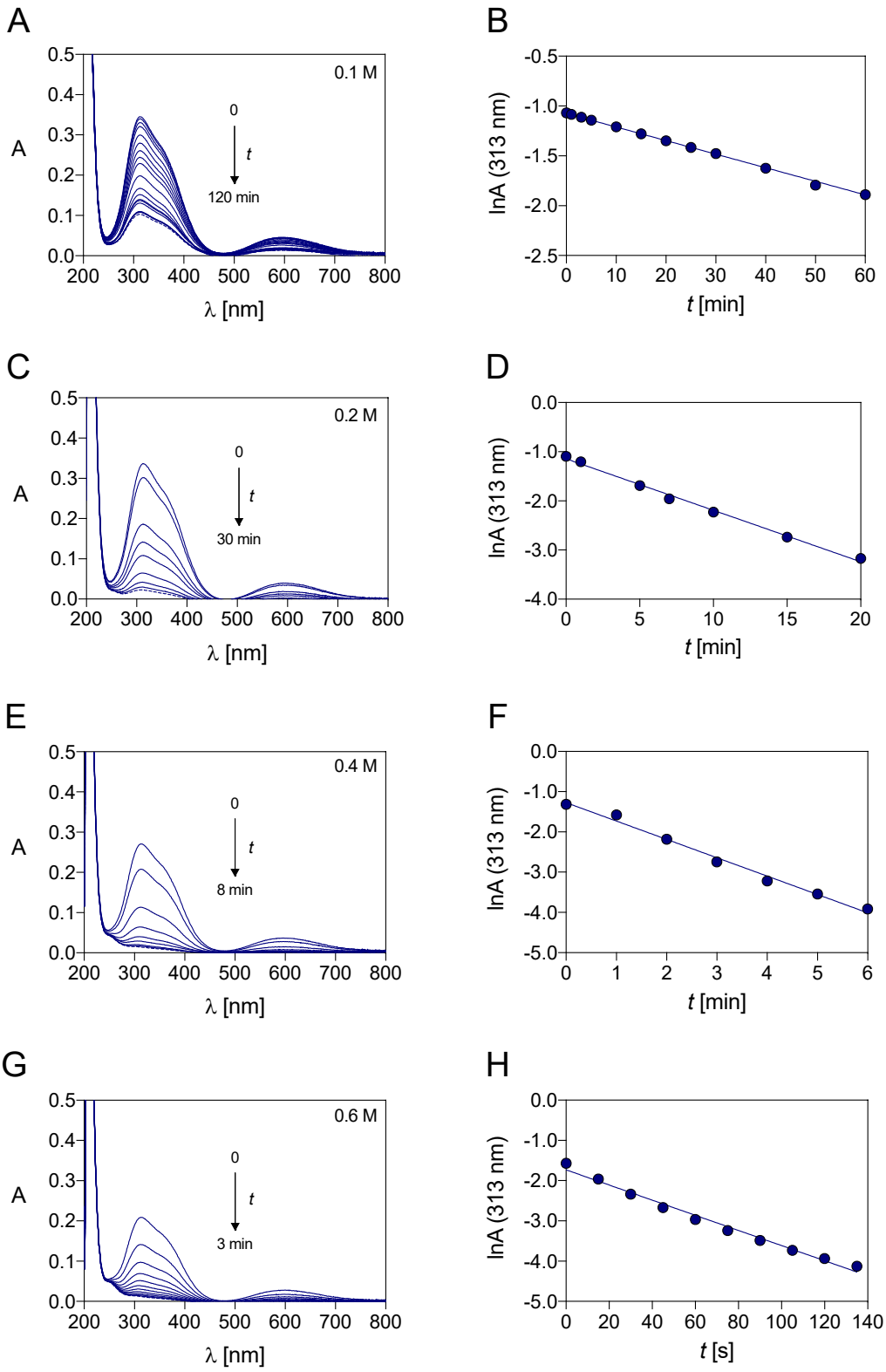

Fig. S27. (A, C, E, G) UV-Vis spectra variation during the acid-assisted decomplexation assays for Cu^{2+}-TRI4S ($C_{Cu^{2+}}$ = C_{TRI4S} = $1.0 \cdot 10^{-4}$ M) at the given (upper right) HCl concentrations (dotted lines correspond to equilibrium conditions). (B, D, F, H) ln*A vs. t* and corresponding fitting line.

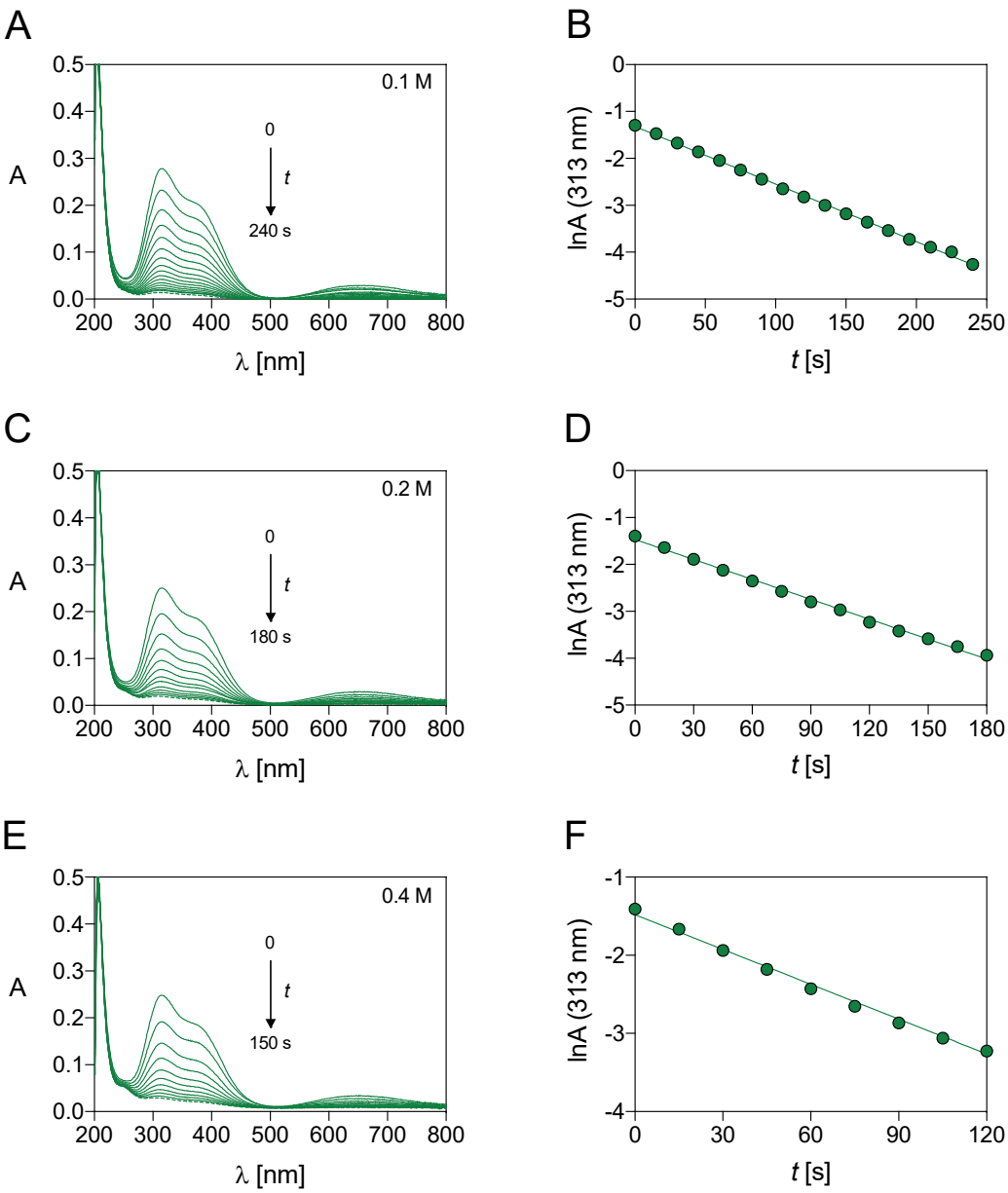

Fig. S28. (A, C, E) UV-Vis spectra variation during the acid-assisted decomplexation assays for Cu^{2+}-TE4S ($C_{Cu^{2+}} = C_{TE4S} = 1.0 \cdot 10^{-4}$ M) at the given (upper right) HCl concentrations (dotted lines correspond to equilibrium conditions). (B, D, F) ln*A vs. t* and corresponding fitting line.

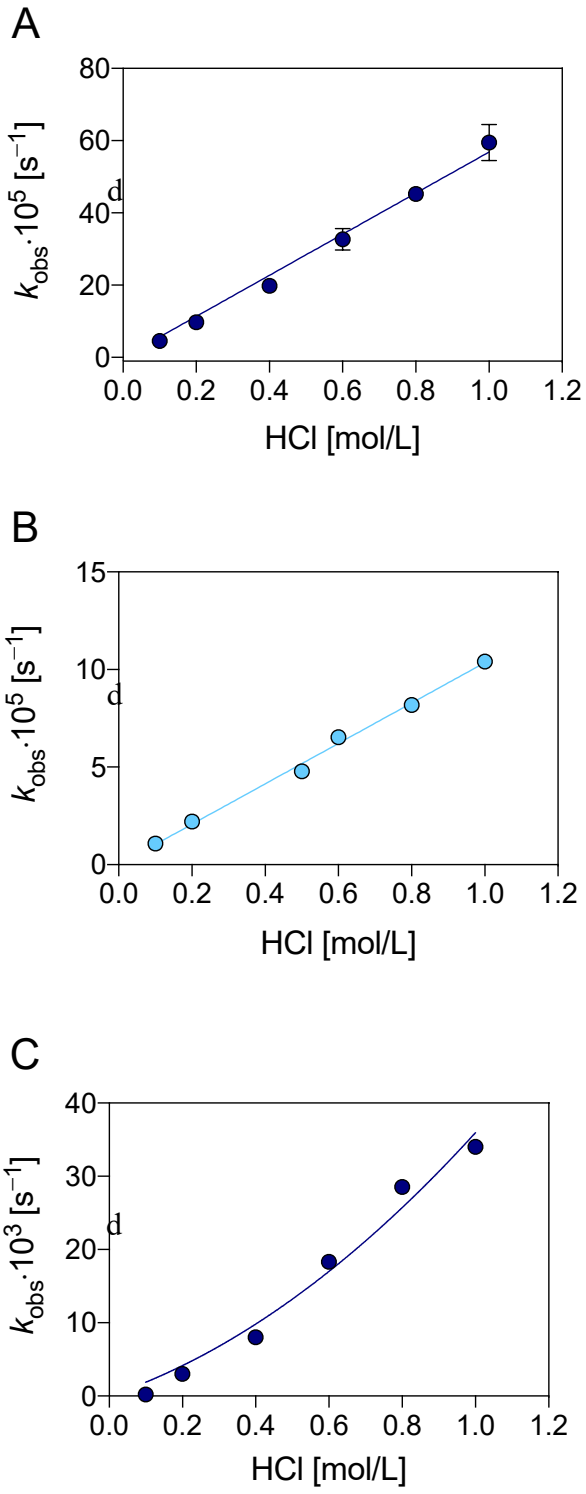

Fig. S29. pH-Dependence of ${}^{d}k_{obs}$ for acid-mediated decomplexation of the Cu^{2+} complexes with (A) DO4S, (B) DO2A2S and (C) TRI4S at room temperature, and corresponding fitting lines obtained with the equation ${}^{d}k_{obs} = {}^{d}k[H^+]$ (for DO4S and DO2A2S) or ${}^{d}k_{obs} = {}^{d}k\,[H^+] + {}^{d}k_2\,[H^+]^2$ (for TRI4S).

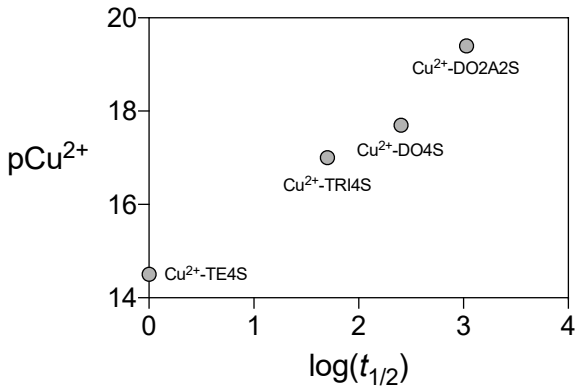

Fig. S30. Correlation between pCu^{2+} values at pH = 7.4 and $\log(t_{1/2})$ at pH = 1.

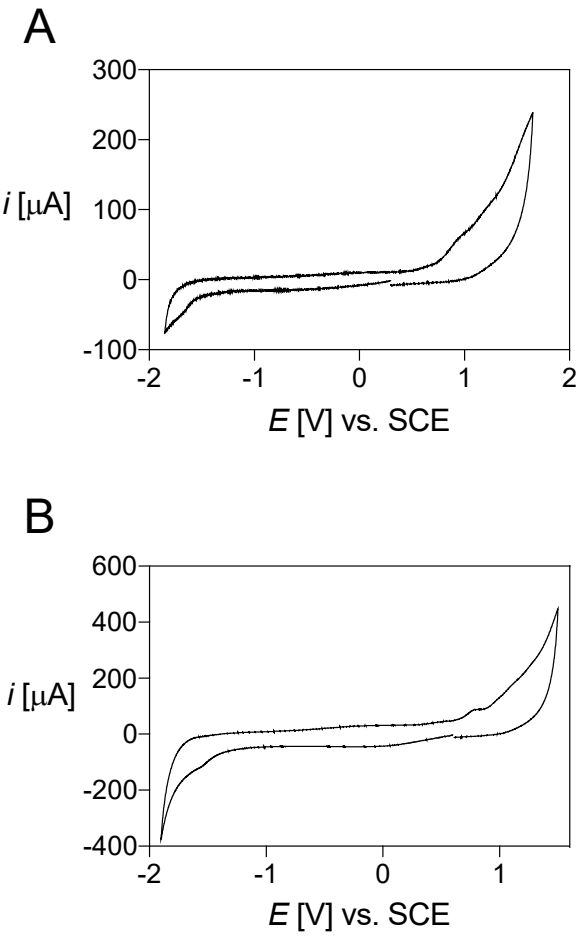

Fig. S31. Cyclic voltammograms of free (A) TRI4S (C_{TRI4S} = $9.85 \cdot 10^{-4}$ M) and (B) TE4S (C_{TE4S} = $8.80 \cdot 10^{-4}$ M) in aqueous solution, I = 0.15 M $NaNO_3$ and T = 25 °C acquired at a scan rate of 0.1 V/s.

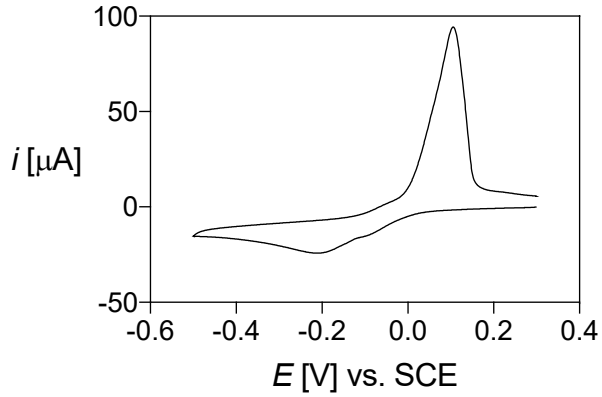

Fig. S32. Cyclic voltammogram of unbound Cu^{2+} ($C_{Cu^{2+}}$ = 2.3·10^{-3} M) in aqueous solution, I = 0.15 M $NaNO_3$ and T = 25 °C, acquired at a scan rate of 0.1 V/s.

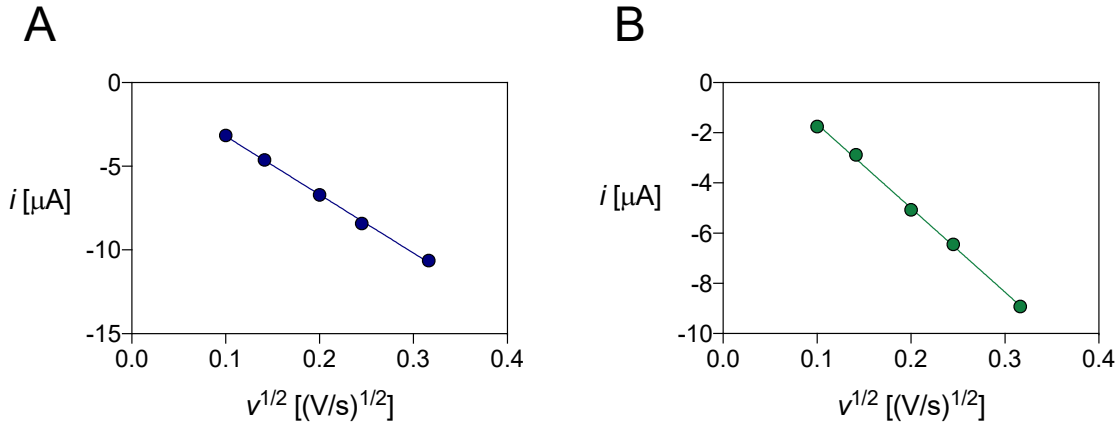

Fig. S33. Variation of the cathodic current (i_{pc}) (see **Fig. 5**) with the square root of the scan rate ($v^{1/2}$) for the Cu complexes of (A) TRI4S and (B) TE4S, and corresponding linear regressions.

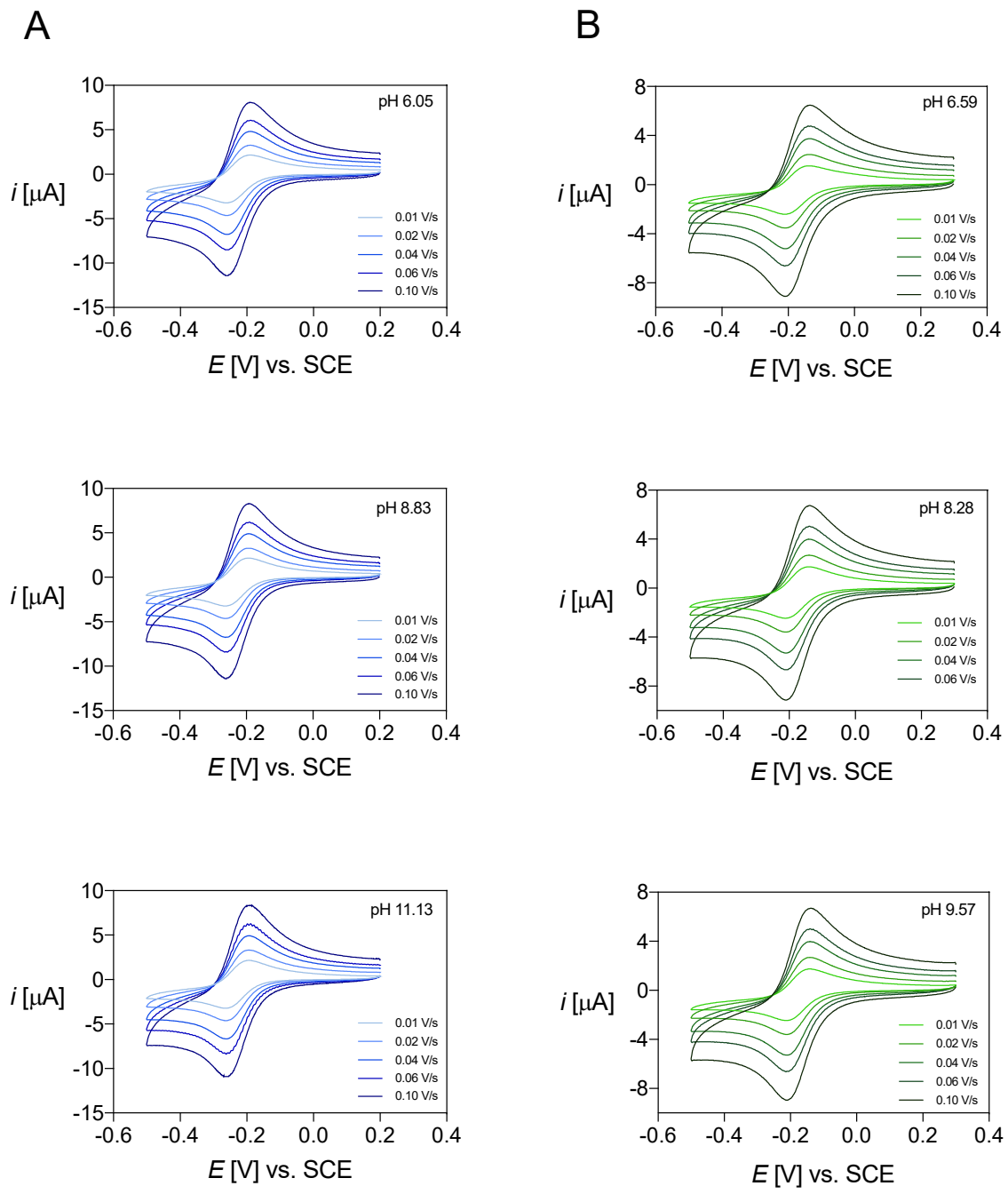

Fig. S34. Representative cyclic voltammograms of the copper complexes of (A) TRI4S ($C_{Cu^{2+}}$ = 8.0·10^{-4} M, C_{TRI4S} = 1.0·10^{-3} M) and (B) TE4S ($C_{Cu^{2+}}$ = 8.0·10^{-4} M, C_{TE4S} = 1.1·10^{-3} M) in aqueous solution at different pH (upper right), I = $NaNO_3$ 0.15 M and T = 25 °C acquired at different scan rates.

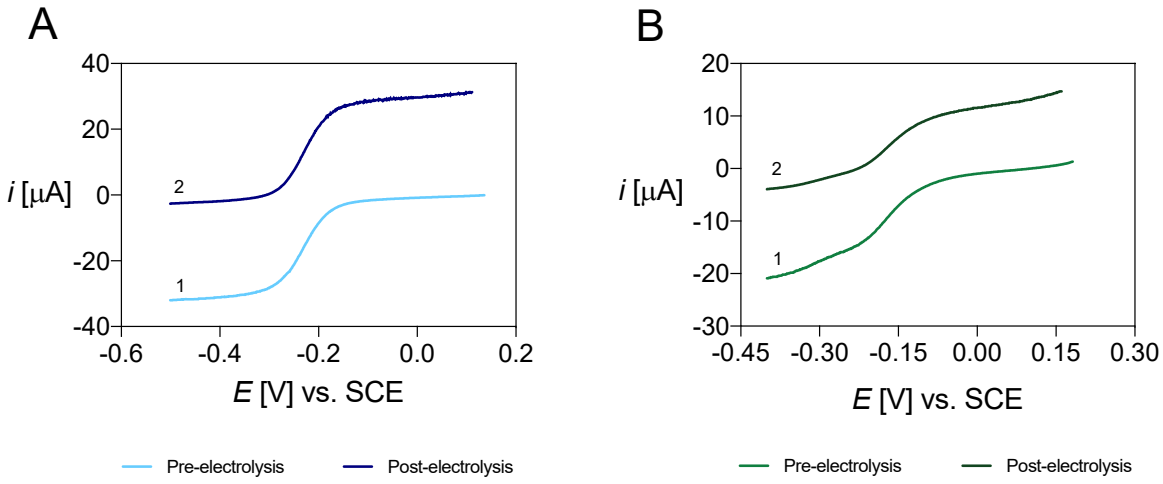

Fig. S35. LSV of (A) Cu-TRI4S (C_{Cu} = 8.0·10^{-4} M, C_{TRI4S} = 1.0·10^{-3} M) and (B) Cu-TE4S (C_{Cu} = 6.0·10^{-4} M, C_{TE4S} = 7.0·10^{-4} M) before ("1") and after ("2") electrolysis at (A) −0.45 V and (B) −0.40 V, performed with a rotating disk electrode at ω = 2000 rpm and v = 0.005 V/s, with I = 0.15 M $NaNO_3$ and T = 25 °C.

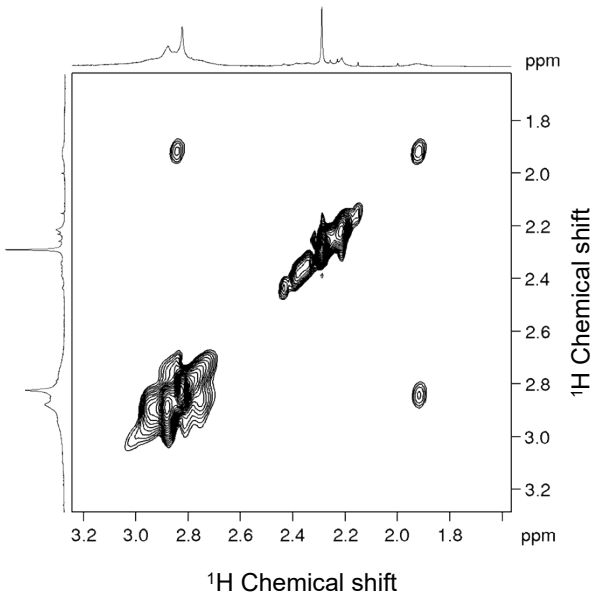

Fig. S36. TOCSY spectra of Cu^{+}-TE4S at pH 8 (C_{Cu} = 6.0·10^{-4} M, C_{TE4S} = 7.0·10^{-4} M) (see also caption of **Fig. 6**).

Supplementary References

1 M. Tosato, M. Dalla Tiezza, N. V. May, A. A. Isse, S. Nardella, L. Orian, M. Verona, C. Vaccarin, A. Alker, H. Mäcke, P. Pastore and V. Di Marco, *Inorg. Chem.*, 2021, **60**, 11530-11547.